MANIPULATION OF PARTICLES USING INERTIAL MICROFLUIDICS AND VISCOELASTIC FLUIDS

A THESIS SUBMITTED TO
THE GRADUATE SCHOOL OF ENGINEERING AND SCIENCE
OF BILKENT UNIVERSITY
IN PARTIAL FULFILLMENT OF THE REQUIREMENTS FOR
THE DEGREE OF
MASTER OF SCIENCE
IN
MATERIALS SCIENCE AND NANOTECHNOLOGY

By
Mohammad Asghari
March 2018

Manipulation of Particles Using Inertial Microfluidics and Viscoelastic Fluids
By Mohammad Asghari
March 2018

We certify that we have read this thesis and that in our opinion it is fully adequate, in scope and in quality, as a thesis for the degree of Master of Science.

Çağlar Elbüken(Advisor)

Memed Duman

Mehmet Selim Hanay

Approved for the Graduate School of Engineering and Science:

Ezhan Karaşan
Director of the Graduate School

ABSTRACT

MANIPULATION OF PARTICLES USING INERTIAL MICROFLUIDICS AND VISCOELASTIC FLUIDS

Mohammad Asghari
M.S. in Materials Science and Nanotechnology
Advisor: Çağlar Elbüken
March 2018

Recent years have witnessed an elevated trend in using miniaturized and lab-on-a-chip systems in biomedical devices due to numerous advantages including minimal sample/reagent consumption, portability, and superior performance. One of the key challenges within these microsystems is to precisely manipulate and order bio-particles. Various techniques have been introduced to accomplish this mission. Inertial microfluidics enables lateral migration of particles and cells in laminar flow regime due to the velocity gradient effect in moderate Reynolds number. Moreover, viscoelastic fluids exploit intrinsic elastic property of the fluids to transfer particles and cells across laminar flow streamlines. Both methods utilize inherent properties of fluids alleviating any external force field inducer. This dissertation elucidates inertial and viscoelastic effects on particles and cells motion and investigates some unexplored migration behaviors. For inertial migration study, a new fabrication method termed tape'n roll is introduced enabling to study migration in both 2D and 3D structures. To better unravel the covert mechanism of migration, computational model is applied. For viscoelastic behavior study, focusing of particles inside three different viscoelastic fluids in a straight glass capillary tube is scrutinized through optical system and image processing.

Keywords: Microfluidics, Micromanipulation, Inertial fluidics, Viscoelastic fluids.

ÖZET

ATALETSEL MİKROAKIŞKANLAR VE VİSKOELASTİK SIVILAR KULLANARAK PARÇACIKLARIN HİZALANMASI

Mohammad Asghari
Malzeme Bilimi ve Nanoteknoloji, Yüksek Lisans
Tez Danışmanı: Çağlar Elbüken
Mart 2018

Son yıllarda gelişen mikroüretim teknikleri ile birlikte minyatür sistemlerin ve yonga üzeri laboratuvar sistemlerinin kullanımında ciddi bir artış yaşanmaktadır. Bu sistemler geleneksel sistemlere göre çok düşük miktarda örnek, solüsyon gerektirmekte, taşınabilir olmakta ve daha hassas ölçüm imkanı sağlamaktadır. Bu sistemler için en önemli uygulamalardan bir tanesi de bio-hparçacıkların hassas şekilde hizalanmasıdır. Bu amaçla çok farklı teknikler geliştirilmiştir. Ataletsel mikroakışkan sistemler bu amaçla geliştirilen sistemler arasında öne çıkmaktadır. Bu yöntemde parçacıklar kanal profilindeki sıvı akış hızı değişiminden dolayı orta miktardaki Reynolds sayısındaki akış rejimlerinde sıvı içinde hizalanmaktadır. Buna ek olarak sıvıların viskoelastik özelliklerinden faydalanılarak da parçacık hizalanması mümkündür. Bu her iki teknik için de sıvı ve akışın kendi özellikleri kullanılmakta ve başka bir mekanizmaya ihtiyaç duyulmamaktadır. Bu tez ataletsel mikroakışkan ve viskoelastik etki kullanılarak parçacık ve hücre hizalanması üzerinedir. Ataletsel mikroakışkan sistemler için yeni bir üretim tekniği geliştirilmiştir. Yapıştır-döndür ismini verdigimiz bu teknikle hem 2 boyutlu hem de 3 boyutlu mimariler üretilebilmektedir. Ayrıca parçacık hizalanmasının detaylı analizi için hesaplamalı bir bilgisayar analiz modeli geliştirilmiştir. Viskoelastik etki ile parçacık hizalaması için üç farklı viskoelastik sıvı kullanılarak cam kapiller içinde optik hizalama analizi gösterilmiştir.

Anahtar sözcükler: Mikroakışkan, Mikrohizalama, Ataletsel akışkanlar, Viskoelastik sıvılar.

Acknowledgement

First and foremost, I would like to express my deepest gratitude to my advisor, Dr. Caglar Elbuken, for all his advice, guidance, and insdispenable support. My master's study would have been very laborious and grey without him and I am extremely delighted to be mentored by him.

I would like to sincerely thank and appreciate my jury members, Dr. Mehmet Selim Hanay and Dr. Memed Duman, for being as jury member in my MS thesis defense and their helpful suggestions and comments.

I would like to thank my companion, Reza Rasooli, for his invaluable help for developing computational code. Moreover, I would also like to thank Murat Serhatlioglu for his cooperation during fabrication process and experiments . This thesis would be arduous without the help of these two persons. My sincerest thanks go to Dr. Kaitlyn Hood for her generous sharing of inertial lift force codes for microchannels with different aspect ratios. Moreover, I appreciate Dr. Bülend Ortaç and Dr. Mehmet E. Solmaz for their helpful discussion on flow cytometry. I like to extend my appreciation to all the previous and current members of Elbuken Research Group. I would like to thank Ziya Isiksacan, Mustafa Tahsin Guler, Ali Kalantarifard, Ismail Bilican, Resul Saritas, Pinar Beyazkilic, Elnaz Alizadeh Haghighi, Abtin Saateh, Baris Karakus, Pelin Kubra Isgor, and Merve Marcali.

Also, I would like to thank Dr. Mehmet Yilmaz and engineers of clean room for their kind help and instruction on facility usage. I must express my deepest gratitude to Dr. Hasan Guner for helpful discussions on biosensors and optical systems. I kindly like to thank my close friends including Hossein Alijani, Reza Rasooli, Murat Serhatlioglu, Masoud Ahmadi, Soheil Firooz, Latif Onen, and Arsalan Nikdoost for encouraging and supporting me through my studies. Finally, I sincerely thank my lovely family members: my father Ebrahim, my mother Rogayyeh, my brothers Hadi and Hamed for their sincere and endless encouragement and support.

Contents

List of Figures

List of Tables

Chapter 1

Introduction

The ability to precisely control the migration of particles inside microfluidic systems plays critical role for biomedical and industry applications. To date, many methods and tools have been introduced to reach this goal. These methods can be classified in two categories: active method and passive one. In former approach, external force inducers including acoustic, electrical, magnetic, or optical manipulators are exploited. In the latter method, due to the intrinsic property of the fluid and flow condition, particles can be manipulated and ordered. For biomedical chips and point-of-care devices, simplicity of the system plays crucial role and a passive method is preferred. In a passive method, particles can either be influenced by geometry effects like deterministic lateral displacement (DLD) method or by flow conditions and fluid properties including inertial microfluidics and viscoelastic effects.

Inertial microfluidics refers to flow condition in micro scale and laminar flow regime where Reynolds number is non-negligible ($1<Re<200$). As a result, in Navier-Stokes equation, fluid momentum is considered yielding a non-linear and irreversible equation of motion. In other words, the effect of viscosity and inertia of the fluid are both finite. This leads to exertion of considerable inertial lift force in lateral direction to the moving particles inside the microchannel and

can transfer them between the laminar flow streamlines. This interesting phenomenon can be used as a tool for manipulation and ordering of particles inside microchannels without the need for extra component. One of the earliest studies for inertial microfluidics was presented by Di Carlo et al. in 2007[1]. In this work, inertial focusing of particles inside straight, symmetric, and asymmetric serpentine microchannels was reported. Soon after, Bhagat et al. reported continuous particle separation in spiral microchannel using inertial microfluidics[2]. Significantly, these paramount studies led to introduction of further inertial microfluidics platforms by researchers for a large variety of biomedical applications. The key advantages of inertial microfluidics are its simplicity and high throughput where it can be used for detection and isolation of rare cells including circulating tumor cells (CTCs) from the whole blood.

The other passive manipulation of particles can be achieved by using viscoelastic fluids. Viscoelastic fluids are non-Newtonian fluids and they do not obey Newton's law of viscosity. Newton's law of viscosity relates to direct proportionality between shear stress and shear rate where this ratio is viscosity ($\mu=\frac{\tau}{\dot{\gamma}}$) and it is independent of time and shear rate. Viscoelastic fluids share the elastic property of solids and viscous characteristic of liquids. Due to the elastic feature, they can store and recover shear energy resulting in normal stress generation. Unsurprisingly, the normal stress difference in lateral and axial directions, induces elastic lift force to the particles inside these fluids. This force leads to lateral migration of particles as well as stretching of the soft particles inside the medium. Leshansky et al. were the first to report manipulation of particles inside a viscoelastic fluid in micro scale[3]. They showed that particles align in mid-height plane inside rectangular microslit at the outlet. Later, D'Avino et al. illustrated capability of purely viscoelastic effect to focus particles on centerline of the cylindrical microchannel[4]. Moreover, Yang et al. investigated combination of inertial and viscoelastic effects on migration of particles inside a microchannel with square cross section[5]. The main reasons to use viscoelastic fluids instead of inertial effect of the fluids are the ineffectiveness of the pure inertial lift force for focusing and alignment of small particles (sub-micron) as well as inefficiency of focusing for lower flow rates (Re<1). Therefore, viscoelastic fluids have the potential to

be used for small size particles and even with wide range of flow rates.

This dissertation details physical migration phenomena happening in inertial microfluidics within 2D and 3D structures and viscoelastic focusing inside various viscoelastic fluids.

Chapter 2 provides an extensive study of particle migration inside 2D and 3D structures. The migration of cells inside spiral and squarel 2D structures is illustrated. This novel structure shows similar focusing efficiency compared to the conventional spiral design. We then introduce a new fabrication procedure called tape'n roll to generate 3D structures. By using such a technique, helical microchannels are easily fabricated and migration behavior of particles and cells inside such structures are explored.

Chapter 3 relates to particle manipulation and focusing inside viscoelastic fluids. We investigated particle focusing efficiency inside three viscoelastic fluids and fully characterized them for the best focusing both experimentally and numerically. This chapter has been reprinted with minor adaptations from "Sheathless Microflow Cytometry Using Viscoelastic Fluids" by Mohammad Asghari, Murat Serhatlioglu, Bülend Ortaç, Mehmet E. Solmaz, and Caglar Elbuken. This article was published in Scientific Reports on 27 September 2017. (doi:10.1038/s41598-017-12558-2).

Chapter 4 outlines remarkable points discovered for inertial microfluidics and viscoelastic fluids in this thesis and then proposes further ideas for future works.

Chapter 2

Inertial Migration of Particles inside Microsystems

Particle manipulation in micro scale is an important topic of research due to its applications in biomedical and clinical research[6, 7, 8, 9, 10]. Confinement and ordering of particles based on their size can be achieved by using extrinsic fields, exploiting the medium's rheological properties, optimizing channel geometry, or a combination of them. The use of external fields such as electrical[11],optical[12], magnetic[13], and acoustic[14] fields has been extensively studied for particle manipulation. More recently, passive particle manipulation approaches have gained traction relying on inertial[15] and viscoelastic[16] effects. Particle manipulation using inertial microfluidics depends mainly on flow condition, and channel geometry. For viscoelastic fluids, on the other hand, rheological properties of the fluid can generate elastic force and affect particle motion[17]. Due to its simplicity and higher throughput, so far inertial focusing has been more commonly studied. Inertial migration of particles has been demonstrated in channels with different structures and cross sections for various purposes including sheathless focusing for flow cytometry[18, 19, 20], obtaining steady interparticle spacing for single cell analysis[21, 22], cell trapping[23, 24], size-based[25, 26, 27], and shape-based[28, 29] separation. Most of these studies investigated particle migration in planar structures using straight[1], spiral[26, 30, 31], and serpentine[1, 32]

microchannels. Curved microchannels create vortices in orthogonal direction of the flow direction thus introduce flexibility for particle manipulation by creating secondary forces. Spiral and serpentine channels have been studied in detail. In former structure, magnitude of the Dean flow changes due to the continuous change in radius of curvature along the microchannel. The latter structure is more complex due to the change in the direction in addition to the magnitude of the secondary flow. To keep both the direction and magnitude constant, one solution is to construct 3D helical structures with constant radius of curvature. Schematic of the curved structures and secondary flow arrows are shown in Figure 2.1.

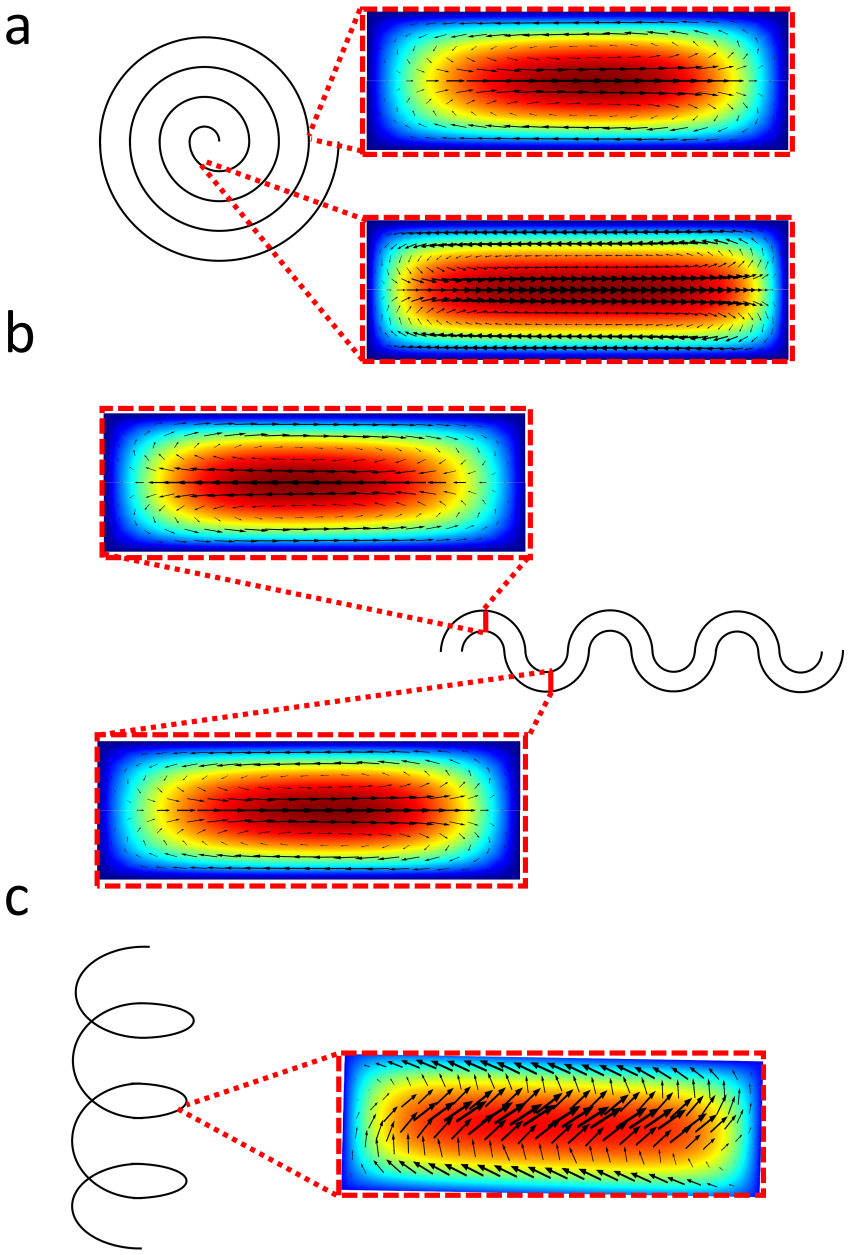

Figure 2.1: Secondary flow arrow field for spiral, serpentine, and helical microchannels. a) For the spiral channel, due to the change in the radius of curvature, secondary flow effect diminishes while particles traveling from inner part to outer part. b) For the serpentine design, due to the change in the direction of curvature, the direction of secondary flow arrow field are reversed while particles are traveling. c) For the helical structure, due to the constant radius of curvature, arrow fields are steady along the microchannel, however, asymmetric arrow field is observed resulted from the helix pitch.

In this chapter, cells migration and focusing in 2D layouts including spiral and squarel microchannels are demonstrated. The squarel design consists of straight channels connected to each other with perpendicular sharp corners spiraling in a loop like manner. Moreover, particle motion inside 3D helical microchannels are analyzed and fully characterized. So far, inertial focusing mostly have been studied experimentally. However, experimental optimization of particle tracking is costly and time consuming. By developing a computational model, it is possible to have better insight for particle motion along the channel. There are only a few studies to computationally analyze particle motion[33, 2, 34, 35, 36]. Here, I have developed a computational method for a thorough understanding of particle motion in 3D helical channel that assists in the design optimization process. This technique has been inspired by the work that has been developed by Reza Rasooli to analyze inertial migration inside spiral and straight microchannels[37].

Results show that particles travel in helical pathways along the channel resulting in an elliptic profile across the channel cross section. The size and the location of the elliptic profile vary based on the parameters affecting the inertial focusing. After optimizing the flow conditions through numerical analysis, experimental analysis is carried out.

In order to produce low-cost 3D helical structures, a novel fabrication method, called "tape'n roll", is presented that uses a microchannel fabricated by conventional soft lithography. The monolithic PDMS microchannel with rectangular cross section was sealed by polyimide tape (Kapton®) and then rolled around a rod, resulting in a helical geometry. The geometrical parameters of the structure (radius of curvature and pitch of helix) can easily be adjusted. "Tape'n roll" method offers many advantages compared to conventional fabrication techniques. It enables the transformation of planar layouts to 3D geometries. Additionally, planar layouts of different cross sections such as square[38], rectangular[39], triangular[40], semi-circular[41], and trapezoidal shapes can be transformed into 3D channels. Helical, spiral and serpentine structures can be produced by using the same straight channel (see Figure 2.2). In materials and methods section, details of this method will be discussed.

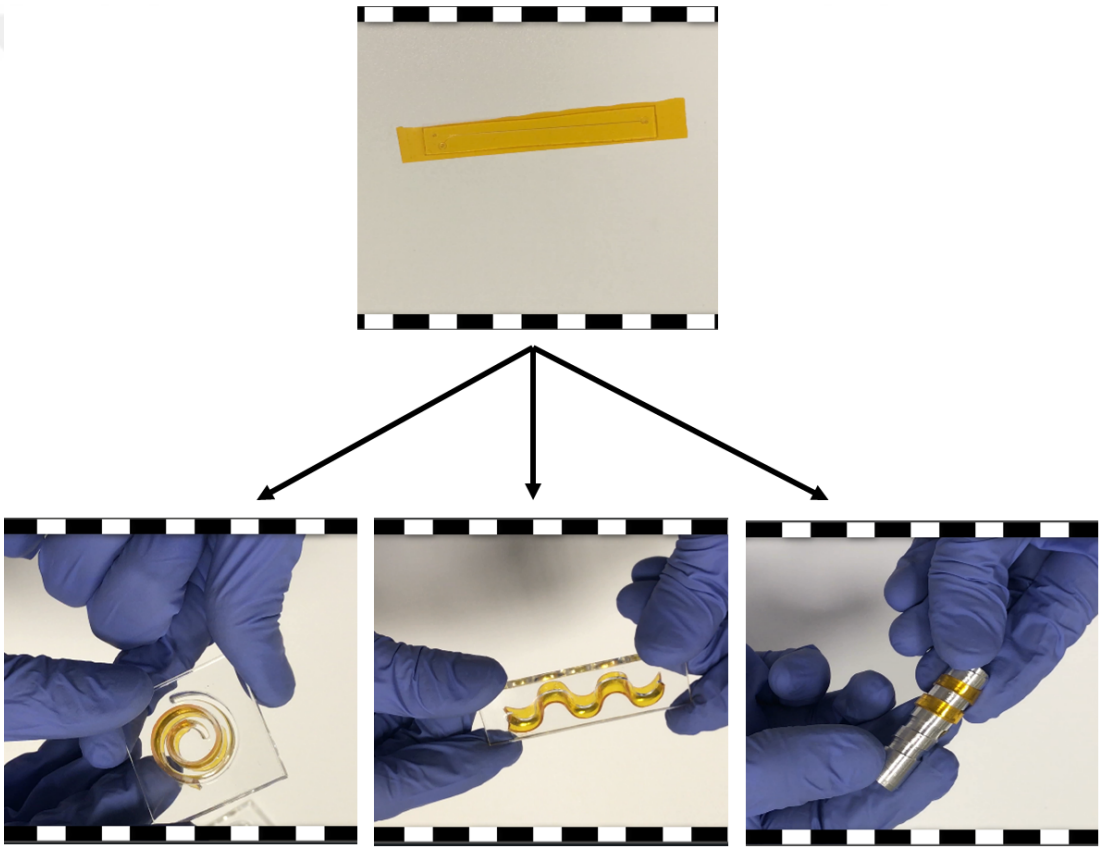

Figure 2.2: "tape'n roll" for obtaining spiral, serpentine, and helical microchannels.

In the case of channel clogging, tape'n roll fabrication offers reusability by simply resealing the microchannel with new tape. Finally, the flexibility of the system allows the fabricated structures to be used in a range of applications including wearable microdevices[42].

2.1 Inertial Microfluidics Theory

Inertial microfluidics studies systems in micro scale where fluid's inertial effects are non-negligible and affect the movement of suspended particles across fluid streamlines. This phenomenon occurs for sufficiently high Reynolds numbers when inertial lift forces for a specific size of particle become dominant, and can transfer suspended particles between the streamlines of the fluid. Two dominant inertial lift forces are shear gradient lift force originating from parabolic flow velocity profile and wall-induced lift force due to the asymmetric flow field around the particle in the presence of the boundaries. The net lift force is the sum of these inertial lift forces and exhibits the potential to be used for particle focusing and separation. The earliest study of inertial effect was investigated by Segre and Silberberg where they showed that rigid particles in a cylindrical pipe migrate to the equilibrium position of an annulus shape with radius of 0.6 times the pipe radius[43]. Lately, implementation of inertial effects in microfluidics has been studied for different geometries. In the simplest shape, for straight channel with square cross section, it was shown that traveling a few centimeters from the inlet, particles migrate to four stable equilibrium positions in the vicinity of the channel wall centers[1, 38]. For rectangle cross section, these equilibrium points collapse to two points near the center of the long walls. Schematic of parabolic velocity profile, inertial shear gradient lift force and wall-induced lift force are illustrated in Figure 2.3a. Moreover, the net lift force field for square (aspect ratio of 1) and rectangular (aspect ratio of 4) are shown in Figure 2.3b. Inertial focusing in channels with different cross sections including triangle and semi-circle was also investigated. It was shown that by combining these geometries in a specific sequence, it is feasible to focus particles in a single train[40]. In all these geometries, the balance between inertial lift forces determines the equilibrium

positions. However, for the separation of particles with different sizes, inertial effects may not suffice since equilibrium positions can be very close to each other. Thus, secondary flows in lateral direction are introduced to separate different size of particles with higher resolution. The resolution of separation is a function of both inertial lift force and Dean drag force resulting from the secondary flows.

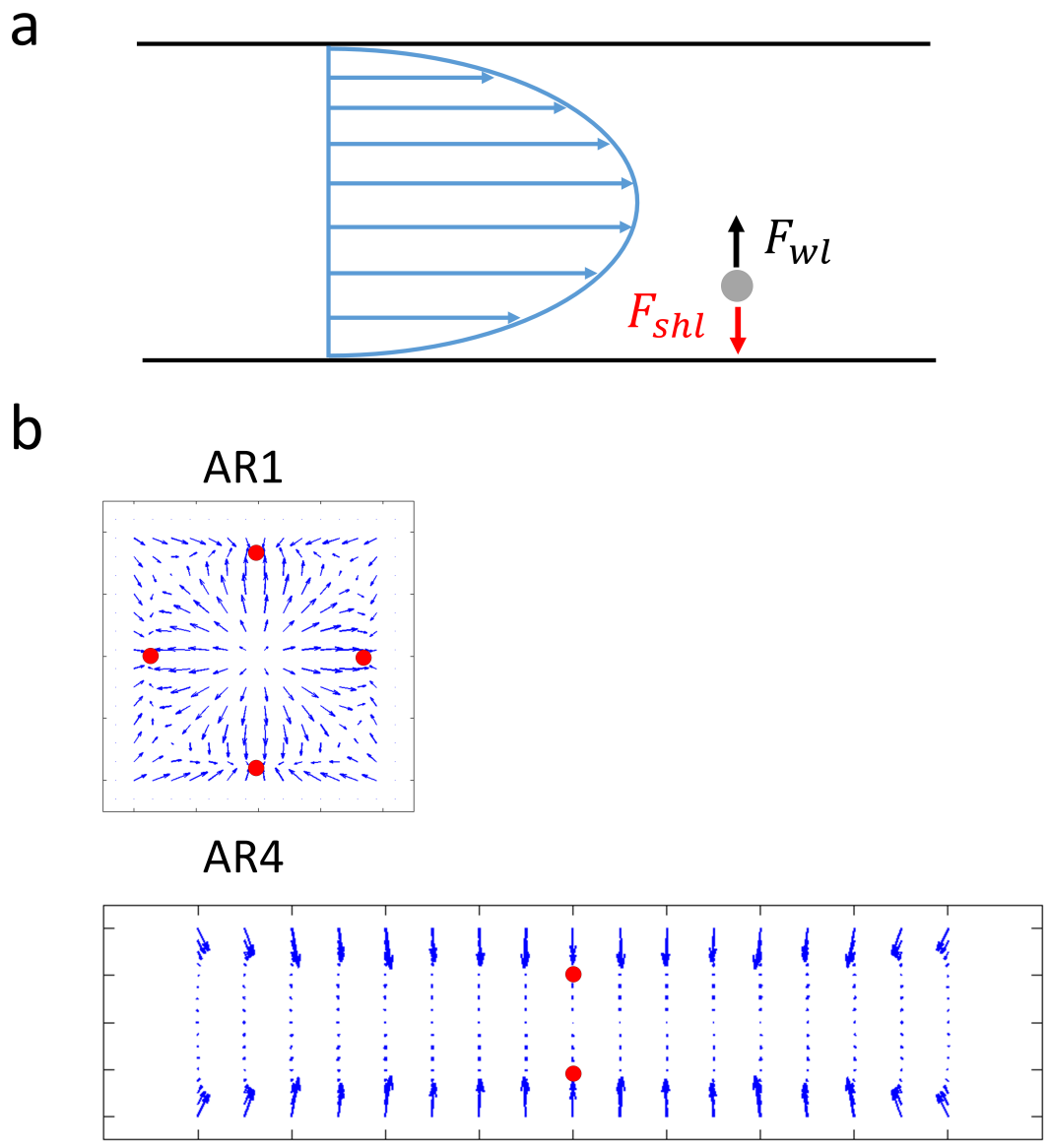

Figure 2.3: a) Illustration of Poiseuille flow profile inside straight microchannel. Due to the sufficiently high Reynolds number, shear gradient lift force (F_{shl}) pushes particle towards the wall. On the other hand, inertial wall-induced lift force (F_{wl}) repels the particle away from the wall due to the asymmetric flow distribution around the particle. b) Net inertial lift force arrows inside rectangular cross sections with aspect ratio (AR) 1 and 4.

To generate secondary flow, curved and microstructured channels (expansion-extraction, micro-pillars, and arc-shaped grooves) have been introduced. Expansion-extraction geometry has been studied extensively. It has been shown that this geometry is capable of separating particles and cells of different sizes[44]. Amini et al. demonstrated the effect of position and number of the pillars on secondary flow transformation and their effect on particle motion[45]. Later, Stoecklein et al. developed a framework to predict inertial flow transformations considering effective parameters[46]. Straight channel with arc-shaped groove arrays is another structure capable of 3D focusing of particles[47]. Curved channels in different formats including spiral[26, 2, 48]and serpentine[1, 32, 35] have been investigated both experimentally and numerically. Curved shape introduces two transverse vortices as secondary flow. The secondary flow is characterized by Dean number which is defined as De=Re$\sqrt{\frac{D_h}{2R}}$ where Re, D_h, and R are Reynolds number, hydraulic diameter, and radius of curvature respectively. To have a constant Dean number along a channel with constant hydraulic diameter and flow rate, radius of curvature should be kept constant. A closed ring shape yields constant Dean number, though it is not practical to implement experimentally. Another option is to fabricate a 3D helical channel with constant radius. However, it is challenging to fabricate 3D structures using conventional microfabrication techniques, especially when at least one dimension of the channels is very small. A figure of merit for a large variety of structures used in inertial microfluidics is shown in Figure 2.4

There are few studies that have investigated 3D channel structures. Paie et al. fabricated all-glass 3D microchannel with straight and curving loops achieving single spot particle focusing using femtosecond laser micromachining[49]. Lee et al. fabricated a helical microchannel using stereolithography based 3D-printer to detect pathogenic bacteria[50]. Xi et al. introduced a novel method of extrusion and curing of PDMS to construct elastomeric microtubes and investigated particle focusing efficiency inside circular microtubes with helical geometry[51].

In this chapter, in addition to 3D channels, cells migration inside spiral and squarel designs are analyzed. To study particle manipulation in 3D structures, a novel fabrication technique is presented to achieve migration of particles in

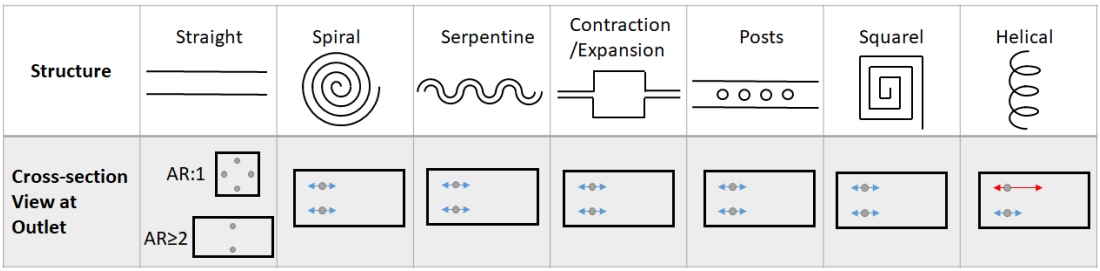

Figure 2.4: Schematic of microchannel designs used for inertial migration studies. For straight channel with square cross section, particles are focused in 4 relaxing points near the center of walls. For rectangular cross section, focusing points decrease to two points near the center of long walls. For all the planar layouts including, spiral, serpentine, contraction/expansion, posts, and squarel, particles are involved in two secondary flow vortices leading to harmonic motion of particles before reaching two focusing points. For 3D helical channel, due to the asymmetric vortices, focusing points act independently.

3D helical channels with rectangular cross section. In addition, a computational method is developed to optimize particle trajectory for 3D helical structures. In the following section, computational modeling is introduced. Afterward, computational and experimental results are discussed.

2.2 Computational Modeling

Particle focusing mechanism can be studied in detail if the particles can be tracked in a given flow field. Experimental approach for particle tracking is very cumbersome and requires registering the particles and capturing their cross-sectional position at several locations along the channel. As an alternative, computational modeling provides the trajectories for particles and allows thorough analysis of focusing performance. However, since the ratio of channel length to hydraulic diameter is high, it requires considerable computational cost to track finite size particles. To overcome this problem, one solution is to simulate a portion of the channel and project the results to the remaining portion by using periodic boundary conditions. Here, an alternative method is proposed to investigate particle migration inside the whole microchannel. First, the geometry is sketched in a 3D

CAD software (Solidworks) and imported to a finite element modeling software (COMSOL) to solve the flow field in the whole channel in the absence of suspended particles. Then, the flow velocities from COMSOL are fed to a MATLAB algorithm, using COMSOL-MATLAB link, and the position of the particles were traced iteratively to obtain particles' trajectory. Here, it is assumed that particles are point particles. Particle-particle interactions and flow field disturbances due to particle motion are not considered. The Lagrangian discrete phase model was used to determine particle trajectory based on the geometry of the channel and exerted forces. By using Newton's second law, force balance equation for a single particle can be written as:

$$\Sigma F = m_p a_p \tag{2.1}$$

where m_p, a_p, and F are particle mass, acceleration, and the forces acting on the particle. For a particle moving inside Newtonian fluid and in inertial regime, the effective forces are: inertial lift force (F_L) due to the sufficiently high Reynolds number, drag force (F_D=$6\pi\mu R_p(u_f$-$u_p)$), buoyancy (F_B=$(\rho_p$-$\rho_f)V_p$g) originating from density difference between fluid and particle, and virtual mass force due to acceleration difference between particle and fluid (F_v=$\frac{1}{2}\rho_f V_p(a_f$-$a_p)$). Here, Stokes drag force is considered for two reasons. First, particle lateral velocity is low enough resulting in small Reynolds number in lateral direction. Second, particle initial velocity is considered the same as the fluid velocity to neglect the particle slip. For lift force, several analytical expressions have been developed[34, 36, 52]. Recently, Hood et al. derived inertial force function for rectangular channels with different aspect ratios by using asymptotic theory. It was verified experimentally by using sub-pixel accurate particle tracking and velocimetric reconstruction of the depth dimension for rectangular channel with aspect ratio (AR) of 2[53]. Here, Hood's lift force is implemented for AR of 1, 2, 4 and 8 [34, 53, 54, 55, 56, 57]. By simplifying all the effective forces in equation (1), we can reach to:

$$a_p = \frac{2}{(2\rho_p + \rho_f)V_p}\left[F_L + 6\pi\mu R_p(u_f - u_p) + (\rho_p - \rho_f)V_p g + \frac{1}{2}\rho_f V_p a_f\right] \tag{2.2}$$

The first step in determining the particle trajectory computationally is to solve for the flow field. For steady-state, incompressible, and laminar flow, continuity and momentum equations can be simplified to:

$$\bigtriangledown.(u) = 0 \tag{2.3}$$

$$\rho(u.\bigtriangledown)u = \bigtriangledown.\big[-pI + \mu(\bigtriangledown u + (\bigtriangledown u)^T)\big] \tag{2.4}$$

where ρ, u, p and μ are fluid density, velocity, pressure, and viscosity, respectively. To solve for the flow field, triangular meshes with sizes varying from 0.4 μm to 4 μm were created. Inlet flow rate was varied to study a range of flow rates. Zero pressure and no slip boundary conditions were used for the outlet and the walls, respectively. As it is shown in Figure 2.5a, as opposed to planar structures, secondary flow is not symmetric for 3D helical structure. Due to the asymmetric vortices in z direction, flow field was solved for the whole channel cross section. To solve the differential equation, the fourth order Runga-Kutta technique is used. This method uses four approximations to determine the acceleration in each step resulting in a more accurate solution. The particle tracking algorithm is summarized in Figure 2.5b. k is defined as k=$\frac{du}{dt}$=f(A(t^i),t^i), where A is the function including the lift force, velocity of the fluid (u_f) and the particle (u_p) in step i. Using the initial conditions, acceleration at the beginning of the time step (k_1) can be obtained. By using this value, the position of the particle and the velocity of the particle and fluid at that position can be obtained. Following the process, k_2 can be obtained by using k_1 and the position and velocities in the previous state. This process is repeated to find k_3 and k_4. Finally, by using these four approximated acceleration values, the velocity and position of the particle in the next step (i+1) can be obtained. Therefore, the particle position can be found in each step iteratively. The particle density, fluid density, and time step are set to 1050 kg/m^3, 1000 kg/m^3, and 5 μs, respectively.

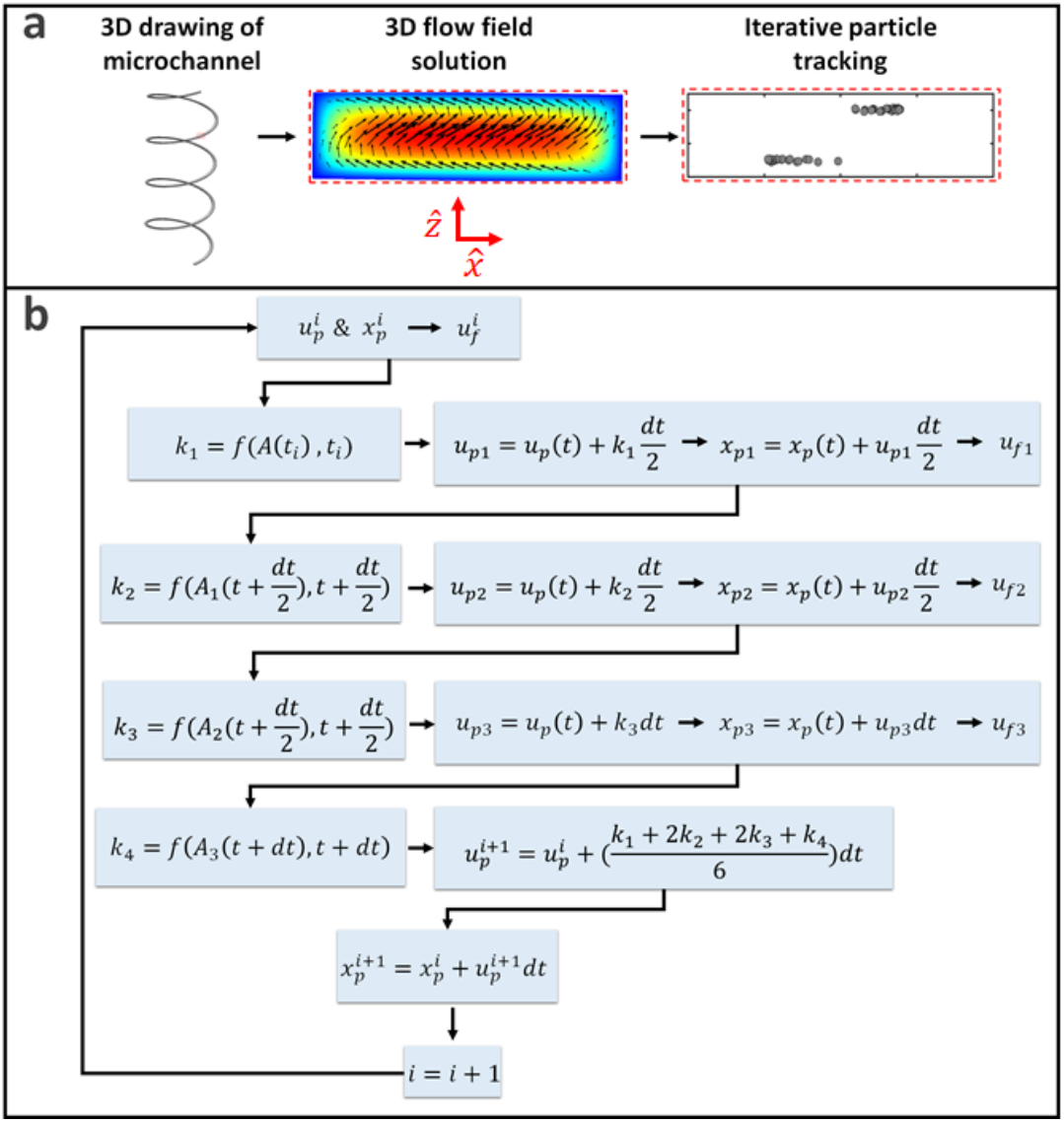

Figure 2.5: a) The computational modeling steps: First, the geometry is sketched using a 3D CAD software. Then, flow field is solved by a finite element modeling software. Finally, the position of the particle along the channel is determined by Lagrangian discrete phase model. b) The particle tracking algorithm: Fourth order Runga-Kutta method is used to find the particle position in each step.

2.3 Computational Results

Here, the particle migration mechanism inside the 3D helical channel is explored. As shown in Figure 2.6, the particles are uniformly distributed at the inlet. As they move along the channel, they get focused and given enough distance they reach to a steady-state focused profile. The focused particle trajectory is an elliptical shape across the channel cross section. Based on the flow condition, geometry, and particle size; the location (d_x, d_z) and the size of the ellipse (R_x, R_z) change, which is analyzed in detail using the computational method.

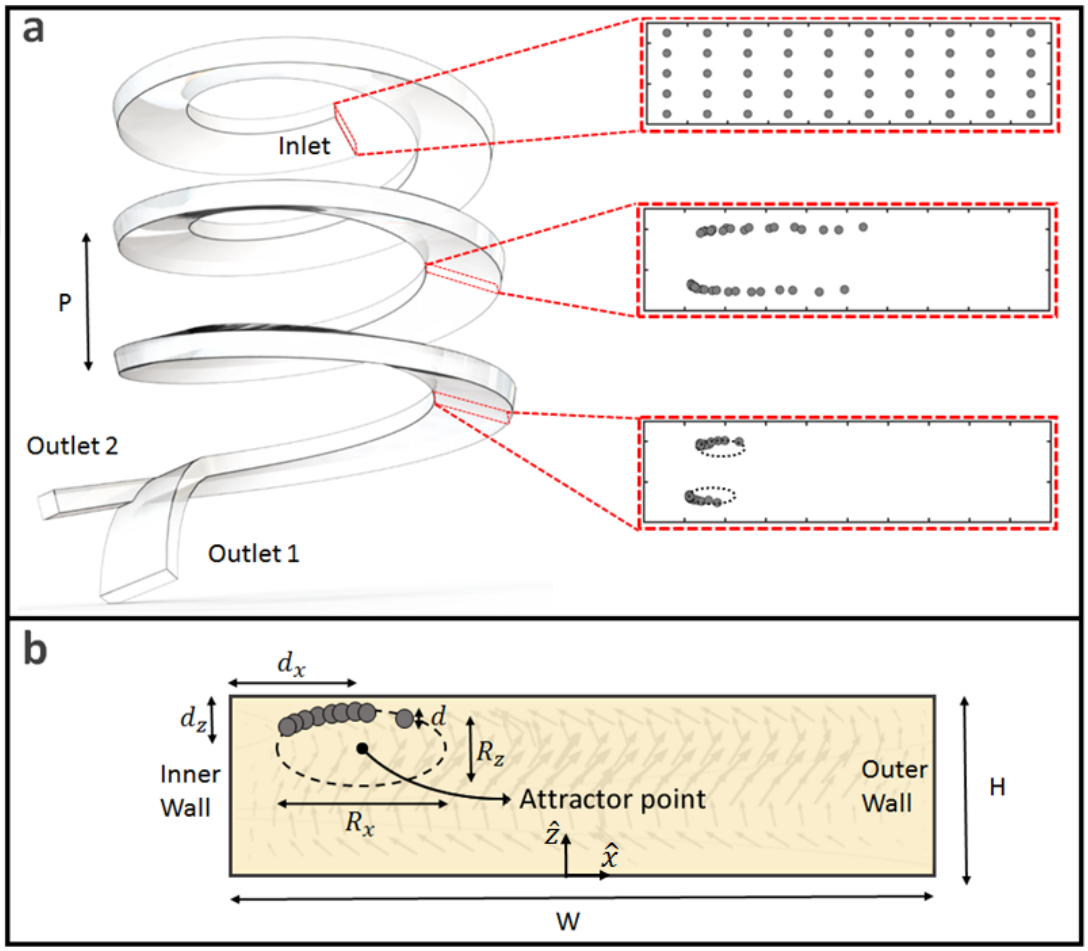

Figure 2.6: The mechanism of inertial migration of particles inside helical channel. a) Uniformly distributed particles are released from the inlet. First, they are focused in two pre-focusing lines due to dominance of inertial forces. Then, they occupy two ellipse shape regions due to the competition of inertial and Dean forces. b) Geometrical parameters of inertial migration for helical channel: P, d_x, d_z, R_x, R_z, H, and W correspond to helix pitch, ellipse center distance from inner wall, distance from upper wall, ellipse diameter in x direction, ellipse diameter in z direction, height, and width of the channel. The arrows in the background illustrate Dean flow field.

2.3.1 Effect of Helix Diameter

Variation of radius of curvature affects the Dean number resulting in the change of the secondary flow. In this section, particles' motion and focusing efficiency using different helix diameter (D) are analyzed. Firstly, single particle motion along helical channel is explored by differing helix diameters. As shown in Figures 2.7a and 2.7b, the particle was released from the same inlet location (x/W=20.8, z/H=0.54), with the same flow rate (Q=40 ml/h). The microchannel has a fixed cross section and pitch (W× H=200× 50 μm^2, P=100 μm) whereas the helix diameter was changed as 2 mm, 8 mm, 14 mm, and 20 mm. The particles are released and tracked along the channel, which has a total length (L) of 80 mm. The particle's longitudinal position from the inlet is represented by l. Similar to the planar spiral geometry, depending on the initial position of the particle, there are two equilibrium positions. In our case, since the particle is released from the upper half of the channel at the inlet, it reaches to an equilibrium at the upper attractor point. For small helix diameter, since the Dean number is high, the particle migrates toward the equilibrium position faster. On the other hand, the Dean flow is strong enough to circulate the particle after reaching the equilibrium position that can be observed for the helix diameter of 2 mm from Figures 2.7a and 2.7b. To better understand the focusing mechanism, the relative force analysis can be considered. From the numerical results, it was observed that the virtual mass force is two orders of magnitude (O$\sim 10^2$) smaller than the lift and Dean forces. Therefore, the competition between the lift force and the Dean force determines the focusing position. The ratio of the inertial lift force to the Dean force for a constant Reynolds number can be scaled as[58]

$$R_f = \frac{F_L}{F_D} \sim \delta^{-1}(\frac{d}{D_h})^3 \tag{2.5}$$

where δ=D_h/D is the curvature ratio (ratio of the hydraulic dimeter, D_h, to the diameter of the curvature, D), and d is the particle diameter. According to this ratio, by increasing D, R_f increases, meaning that F_L becomes dominant. Also, it can be inferred that for straight channel or when helix diameter goes to infinity, particles focus at two equilibrium points near the center of the long

walls. Therefore, it is expected that by increasing the helix diameter, attractor point would drift toward the center near the long wall. It is worth noting that according to Figures 2.7a and 2.7b the particle migrates around the zero lift force line rapidly (Figure 2.7b) and then slowly migrate toward the attractor point in the vicinity of this line.

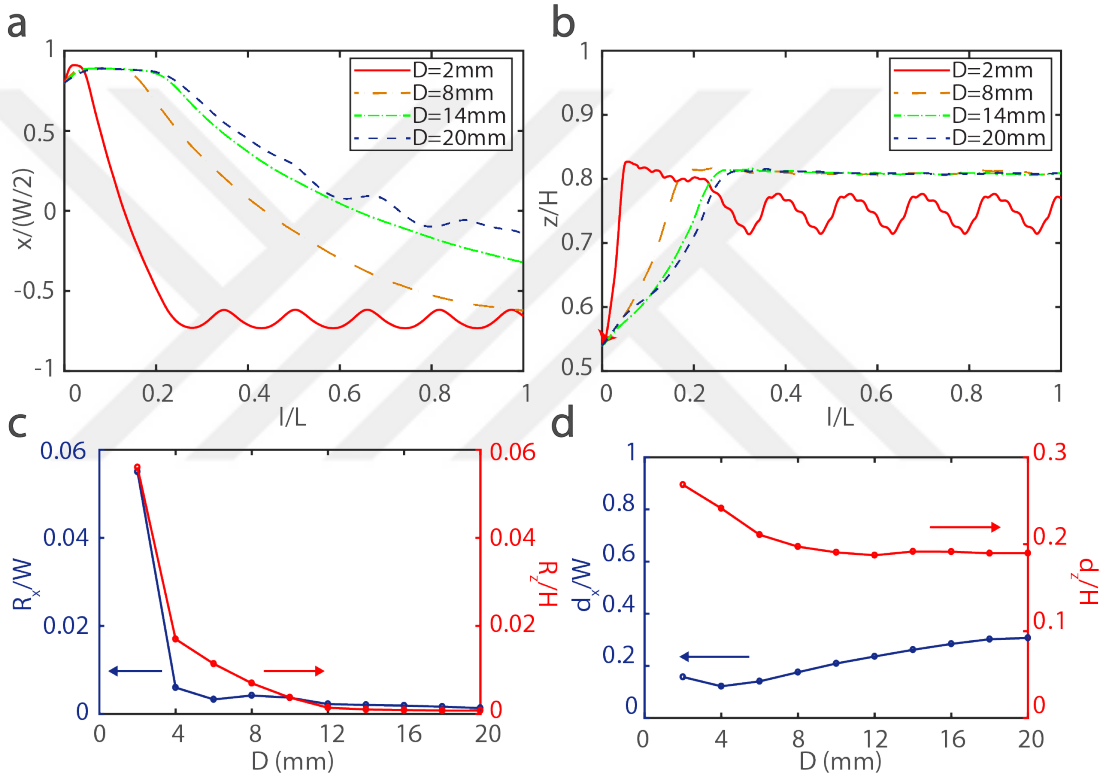

Figure 2.7: Particle trajectory inside 3D helical channel with helix diameters of 2 mm, 8 mm, 14 mm, and 20 mm in a) x-direction and b) z-direction. L is the total length of the channel; l is the particles longitudinal position from the inlet. Steady sate focused particle c) ellipse radii and d) ellipse center (i.e. attractor point) distance from inner and upper walls obtained using multi-particle tracking for changing helix diameter.

To compare the focusing area and focusing distance from the inner and upper wall, multi-particle analysis was performed. This time ten 6 μm diameter particles were released from random positions at the inlet and trajectory calculation was performed for helix diameters from 2 mm to 20 mm with 2 mm increments. As shown in Figure 2.7c, the higher the helix diameter, the smaller the ellipse radii. By increasing the helix diameter, Dean force decreases to be in the same order as the lift force, which results in focusing of the particles in smaller region, however, focusing happens slower compared to helix with smaller diameter. As shown in Figure 2.7d, increasing the helix diameter results in the displacement of the attractor point away from the inner wall toward the upper wall. The position of particles at the outlet for helix diameter of 2 mm, 8 mm, and 20 mm is demonstrated in Figure 2.8.

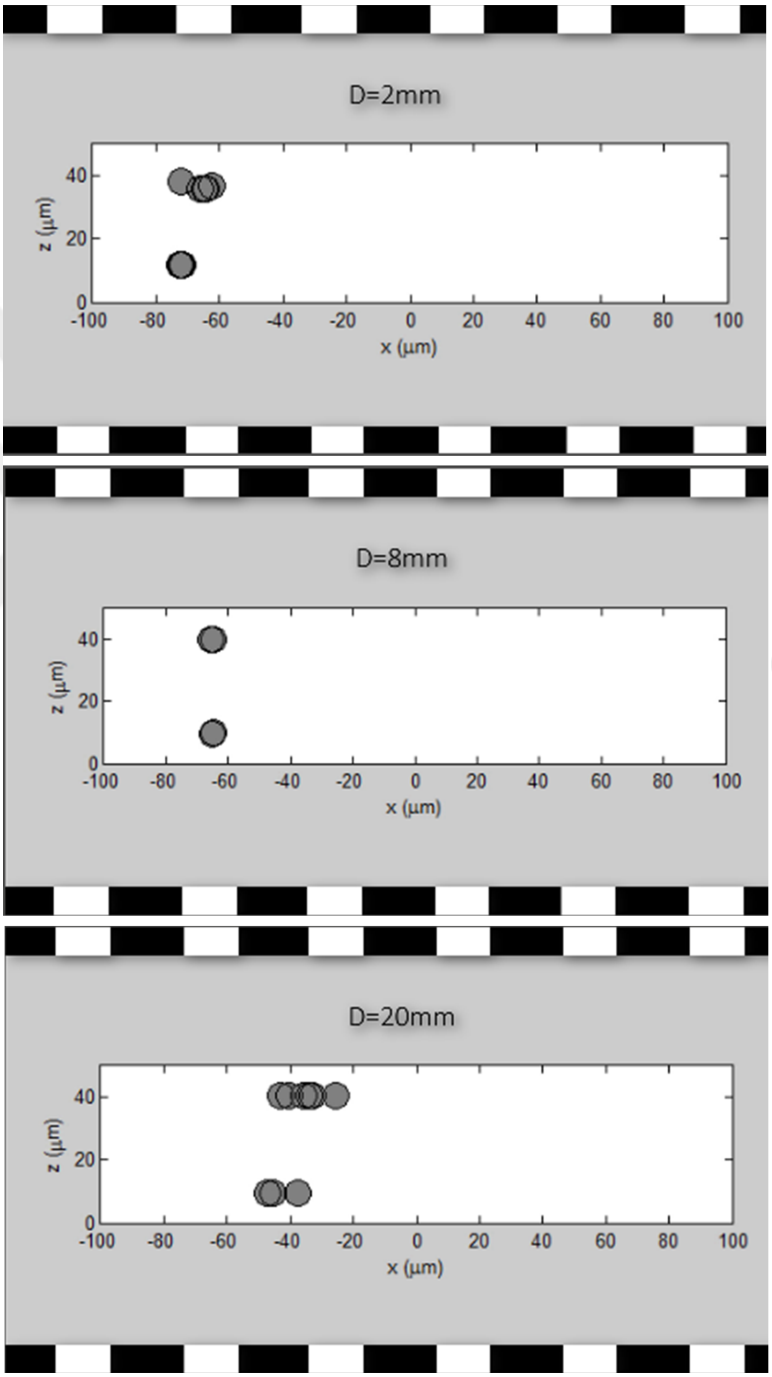

Figure 2.8: Final position of ten 6 μm diameter particles within helix with diameters of 2 mm, 8 mm, and 20 mm. The other parameters are same for all cases (W$\times$ H=200$\times$ 50 μm^2, P=100, and Q=40 ml/h).

2.3.2 Effect of Particle Size

According to equation (2.5), the size of the particle has significant effect on the force ratio. Figure 2.9a represents lateral trajectory of 1 μm, 3 μm, and 6 μm diameter particles released from the same initial position (x/W=20.9, z/H=0.9). The other parameters affecting the particle trajectory were kept constant (W×H=200×50 μm^2, P=100 μm, D=6 mm and Q=40 ml/h). As can be observed, 6 μm diameter particle (a/D_h=0.075) migrates toward the attractor point and stays focused. 3 μm diameter particle (a/D_h=0.0375) travels toward this point but continues to circulate in the vicinity of this point. However, 1 μm diameter particle (a/D_h=0.0125) does not focus and is dragged on the Dean vortices. This analysis is in good agreement with the previous studies for curved microchannels[2, 59]. Force analysis can be used to understand focusing behavior. For 6 μm particle, starting from the initial position, the drag and lift forces are in same direction assisting the particle to migrate toward the inner wall. After reaching the half of the channel in x-direction, the lift force changes direction and competes with the drag force; however, the magnitude of the drag force is higher than the lift force, forcing the particle to migrate toward the inner wall. On the other hand, in z-direction, and specifically near the inner wall, both the drag and lift forces are comparable but in opposite directions resulting in the focusing of the particle in z-direction. Therefore, particle becomes stable near the inner wall. However, for 1 μm particle, the Dean drag force is dominant in both directions along the particle's path, resulting in the migration of the particle on the vortex. To evaluate the focusing efficiency and attractor point position, a multi-particle trajectory calculation was performed. The analysis was done for 10 particles released from the inlet. The particle diameter was changed as 1 μm, 2 μm, 4 μm, and 6 μm for successive runs. Increasing the particle size results in smaller R_x and R_z, and therefore smaller focusing region as depicted in Figure 2.9b. Moreover, by increasing the particle size, the ellipse center gets closer to the inner and upper walls as illustrated in Figure 2.9c. Both effects can be seen from Figure 2.9a. 6 μm diameter particle is focused at a single point (red dashed). By decreasing the particle size, the ellipse size increases, and its center moves away from the inner and upper walls. The final frame at the outlet is provided to show

the particle trajectory of fifty 6 μm and 1 μm diameter particles (Figure 2.10).

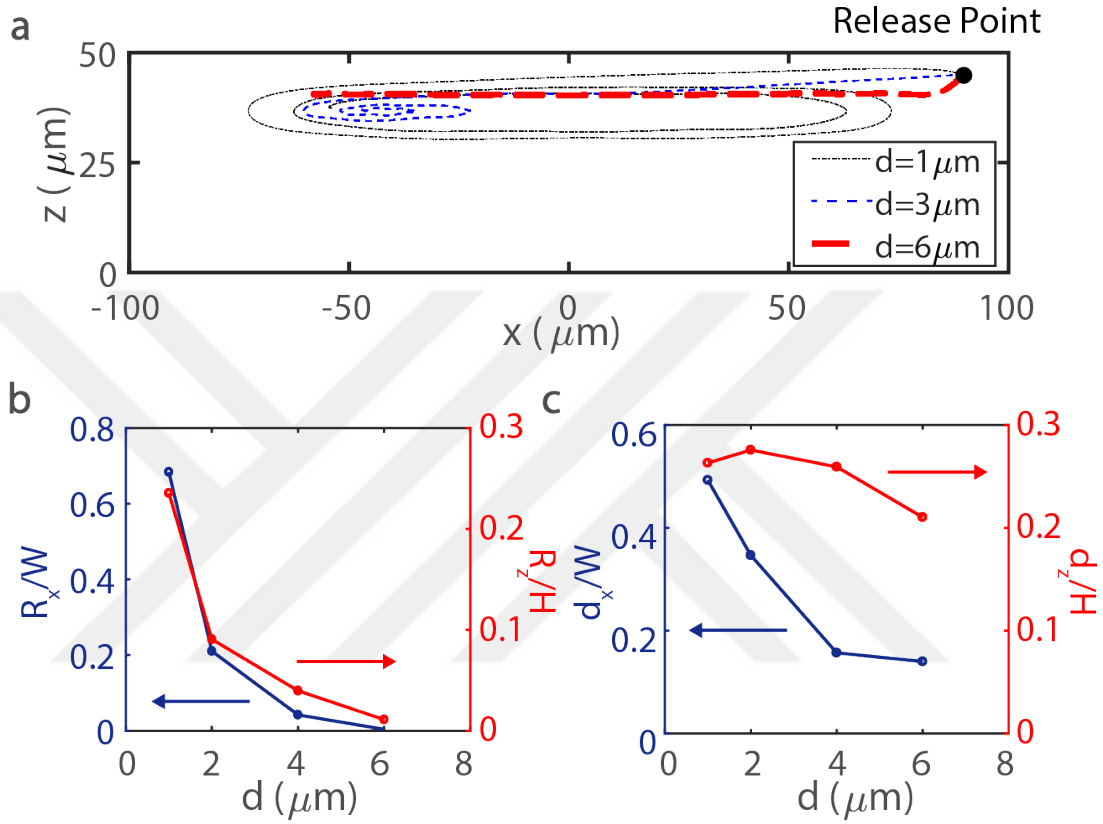

Figure 2.9: a) Cross sectional view of particle trajectory for 1 μm, 3 μm, and 6 μm diameter particles. 6 μm diameter particle migrates and settles at a single equilibrium position. 3 μm diameter particle spirals to the attractor point. 1 μm continues to move in a large elliptic trajectory. b) Ellipse radii and c) ellipse center (i.e. attractor point) distance from inner and upper walls for focused particles obtained using multi-particle tracking for changing particle diameter.

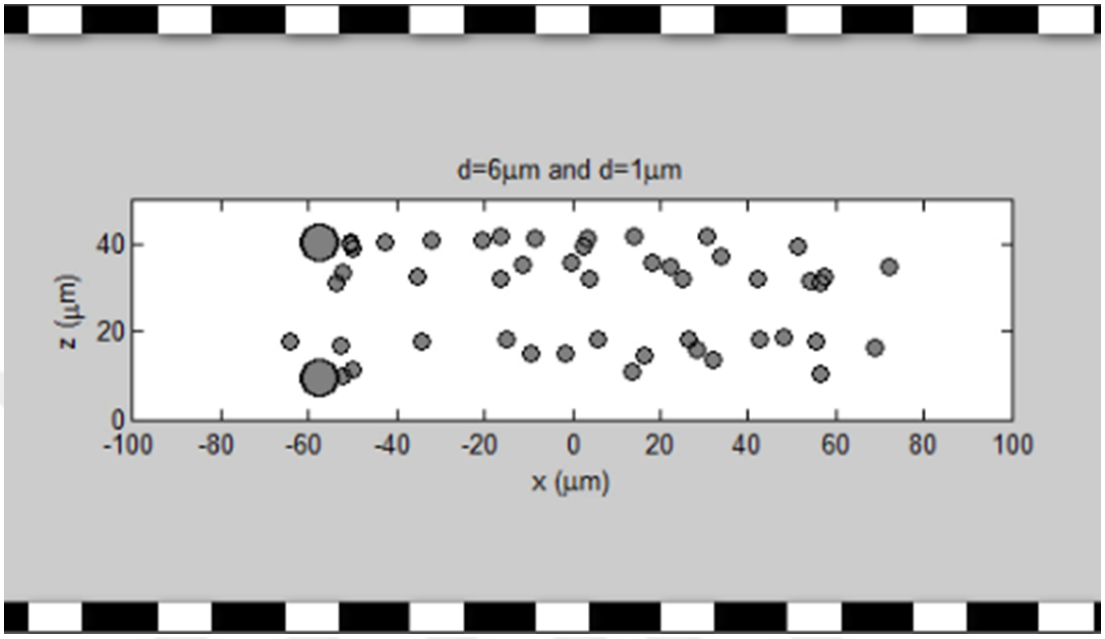

Figure 2.10: Final position of fifty 6 μm and 1 μm diameter particles. The other parameters are same for both sizes (W×H=200×50 μm^2, P=100 μm, D=6 mm and Q=40 ml/h).

2.3.3 Effect of Flow Rate

Flow rate is another parameter that affects the particle focusing. To analyze the focusing performance for varying flow rates, 6 μm diameter particles were studied. Particles were released from the same initial position of x/W=20.8 and z/H=0.54 at flow rates of 20 ml/h, 30 ml/h, 40 ml/h, 60 ml/h, and 80 ml/h. The other parameters were kept the same (W×H=200×50 μm^2, D=10 mm, and P=100 μm). As shown in Figure 2.11a, only for 60 ml/h and 80 ml/h flow rates, particles reach to the stable equilibrium positions. For the lower flow rates, the particles are still travelling to reach stable state for the given channel length. Although the particles are focused in the z-direction on the zero lift force line (Figure 2.11b), they are not focused in the x-direction for smaller flow rates. Therefore, the elliptic trajectory is not created for the low flow rate conditions. To generalize the comparison for all the flow rates, the average distance of the particles' centers from both inner and upper walls are considered (d_x and d_z). Figure 2.11c represents these values for different flow rates. Increasing the flow rate from 20 ml/h to 80 ml/h results in a slight increase in d_x and a decrease in d_z.

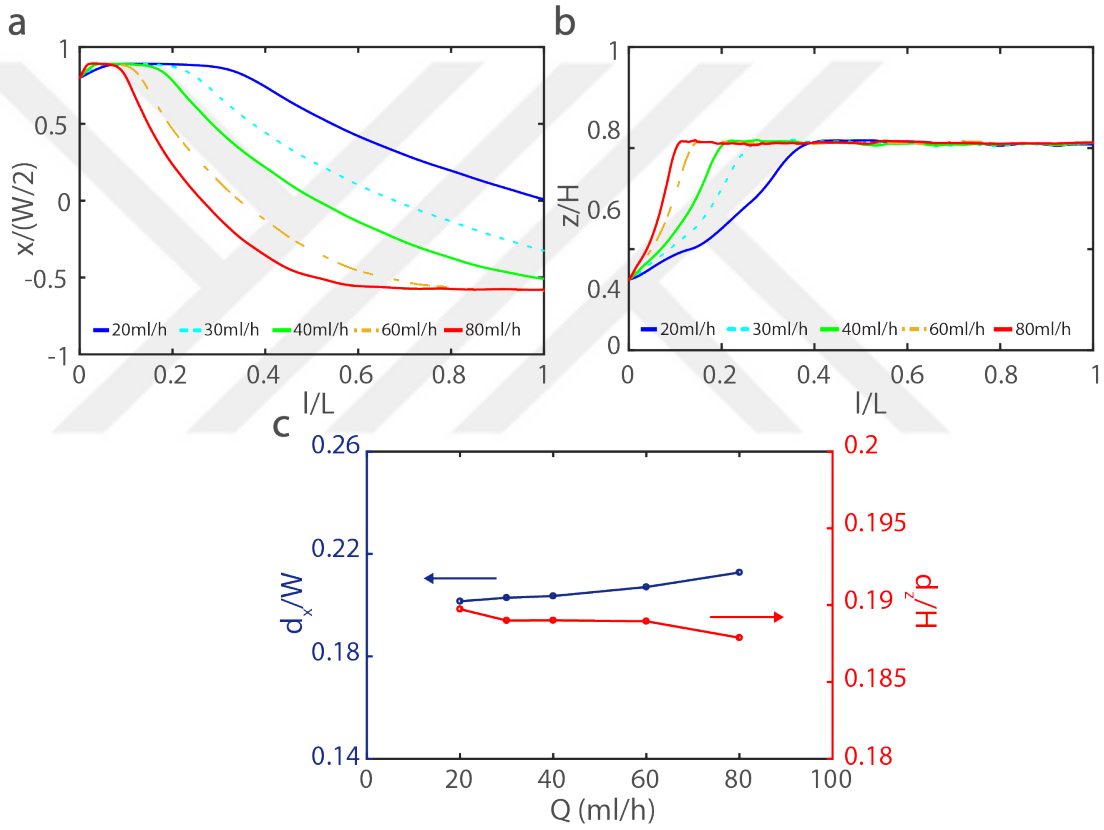

Figure 2.11: Particle trajectory for varying flow rates in a) x-direction and b) z-direction. Increasing the flow rate, enhances the effect of the Dean force, hence the particle moves to the equilibrium position faster. c) Steady sate focused particle ellipse center (i.e. attractor point) distance from inner and upper walls obtained using multi-particle tracking for changing flow rate.

2.3.4 Effect of Aspect Ratio

Particle focusing is also affected by the cross-sectional geometry of the channel. Here, rectangle channels with aspect ratio (AR) of 1, 2, 4, and 8 are considered while other parameters are kept the same (Re=79.35, P=100 μm D=6 mm). Forty particles of 6 μm diameter are introduced from the inlet. Figure 2.12 represents the initial (white circles) and final positions (grey circles) of the particles for varying channel AR. For smaller AR, the particles get focused near the inner wall faster. This is due to the smaller distance that the particles should travel to reach the attractor point in the x-direction. It is interesting to note that the two attractor points are misaligned along the x-direction for low AR. This is explained by higher asymmetry of the Dean vortices for low AR in comparison to high AR structures. Here, the particles are focused in two points with different x positions. Increasing the AR or channel width, results in larger distance for the particle to migrate in the x-direction. It can be observed for AR4 and AR8 cases that the particles are still migrating toward the attractor points. It should be noted that higher AR is suitable for the separation of different size particles and could be utilized in sufficiently long channels.

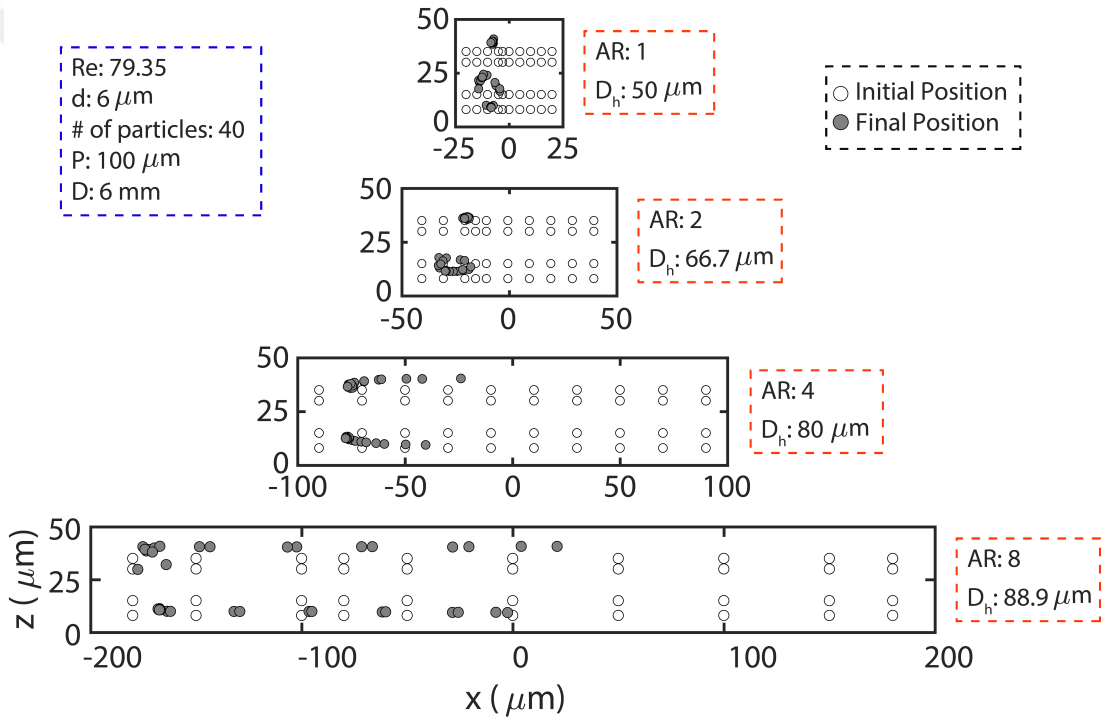

Figure 2.12: The effect of channel aspect ratio on particle focusing. The same Reynolds number and particle size are considered and particle initial (white circles) and final positions (grey circles) are shown. As aspect ratio gets smaller, particles tend to focus at equilibrium position faster. For aspect ratios of 4 and 8, the particles are not settled at equilibrium positions.

2.3.5 Effect of Helix Pitch

Helix pitch is another parameter to affect particle equilibrium state and position. For planar layout where there is no pitch, the Dean flow is symmetric. For the upper and lower half of the microchannel near the zero lift force lines, the fluid flow is toward the inner wall. Based on the balance between the lift force and the Dean force, the equilibrium position changes. However, having a 3D helical channel, i.e. by adding pitch to the structure, the Dean flows become asymmetric. For smaller pitches, this asymmetry effect is not significant to affect the particle motion. However, after sufficiently high pitch value, in the upper half of the microchannel near the zero lift force line, the Dean flow points toward the outer wall resulting in particle focusing far from the inner wall. Figure 2.13 shows the particle trajectory and final status of focusing for different pitch values. As can be observed from Figure 2.13a, for 0.1 mm pitch, 6 μm diameter particles are focused near the inner wall. The two attractor points (for the upper and lower half of the channel) are almost at the same x position. For 4 mm pitch length (Figure 2.13b), there is small misalignment of the particle focusing points. Increasing the pitch to 8 mm (Figure 2.13c) results in the migration of the upper attractor point near the outer wall. Additionally, particles have an oscillatory trajectory in vertical direction for both 4 mm and 8 mm pitches.

For the case of 8 mm pitch and for a particle in the upper left quarter of the channel, the lift force and Dean drag force are both in the same direction and point toward the outer wall. After reaching the upper right quarter of the channel, the lift force changes direction toward the inner wall opposing the Dean force. This competition causes the particles to focus in a point near the outer wall. However, for the particles in the lower half of the channel similar to planar structures, the Dean flow points toward the inner wall, which assists the particle to settle at a point near the inner wall.

These results demonstrate the strength of the computational approach which provide the means to study the influence of all effective parameters in detail. Application of this method to any given geometry would lead to a much faster

design optimization cycle compared to experimental approaches.

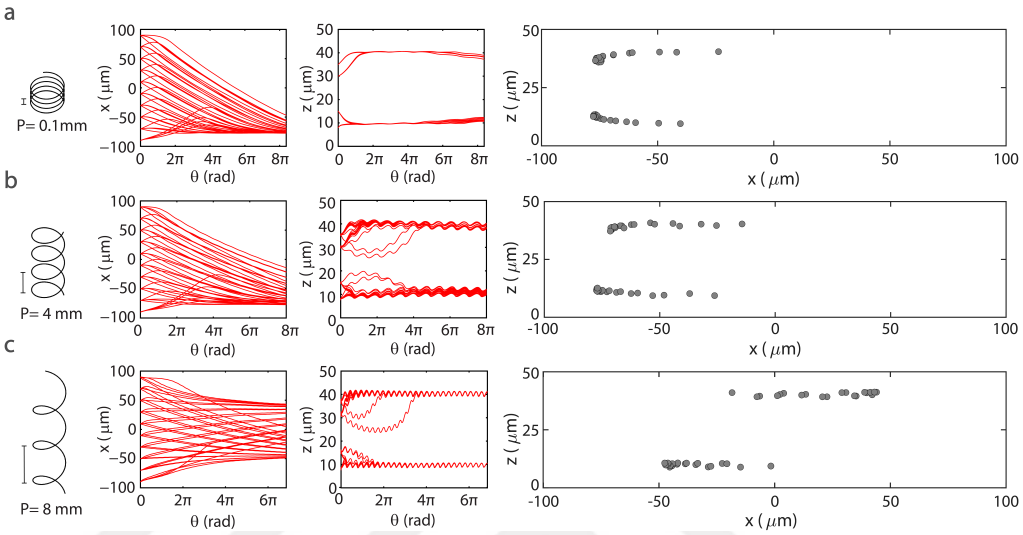

Figure 2.13: Trajectory of the particles for varying helix pitch. The same flow rate (Q=20 ml/h), helix diameter (D=6 mm), particle diamater (d=6 μm), and aspect ratio (AR4) are considered. Helix pitch is changed as a) 0.1 mm b) 4 mm and c) 8 mm.

2.4 Materials and Methods

2.4.1 Chip Fabrication

PDMS soft lithography is a common method used for the fabrication of microfluidic structures[60, 61]. Here, we introduce a novel method to convert the microfluidic structure obtained by soft lithography to a 3D helical shape. For planar layouts (spiral and squarel), the mold is fabricated on silicon wafer in one-step photolithography process. However, for helical microchannel, a two-step photolithography process is used to obtain a step-like channel structure with changing channel depth. Mold designs for fabrication of these microchannels are shown in supplementary figures (Figure A.1 and Figure A.2). In this thesis, separation of particles is not investigated. However, to show the capability of the introduced fabrication technique for separation and filtration purposes, two stage microchannel is fabricated. First, the initial layer with 50×50 μm^2 cross-section was created. Then, 80 mm long, 50×200 μm^2 cross-section main channel was formed on the first layer (Figure 2.14a). SU-8 2050 photoresist (Microchem Corp.) was used for both layers. The 50 μm channel height for the first layer was obtained by spinning the photoresist at 3000 rpm for 40 s. For the second layer, 200 μm channel height was reached by spinning the photoresist at 1000 rpm for 40 s. UV exposures were completed with doses of 180 mJ/cm^2 and 250 mJ/cm^2, respectively. After the post baking process (first layer: 65 °C for 3 min, 95 °C for 10 min, and 65 °C for 2 min; second layer: 65 °C for 15 min, 95 °C for 45 min, and 65 °C for 10 min) followed by 7 min development, the mold fabrication was completed.

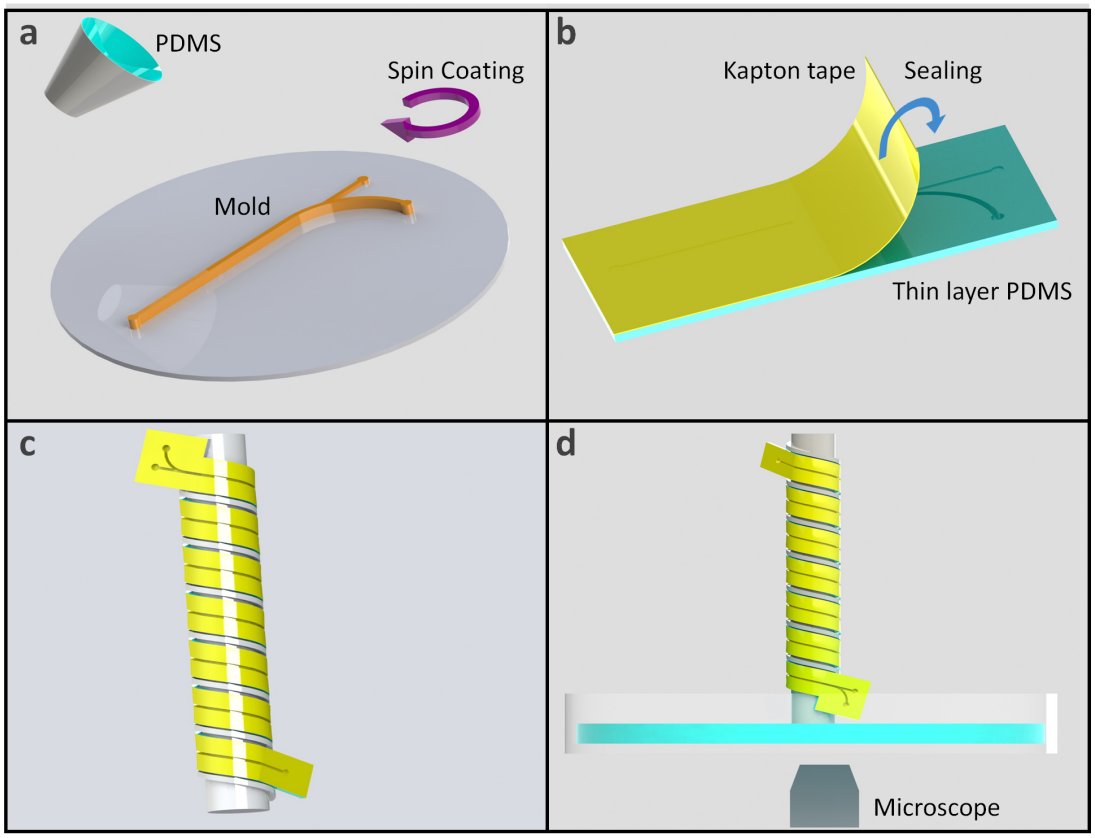

Figure 2.14: Schematic of "tape'n roll" fabrication: a) PDMS is poured on the mold and spin-coated to a uniform thickness. b) The excess PDMS is cut and the channel is sealed with polyimide tape. c) The sealed structure is rolled over the base rod that has helical grooves. d) For side-view microscopic imaging at the channel outlet, the system is fixed vertically on a petri dish by PDMS curing.

The remaining fabrication steps are schematically illustrated in Figure 2.14. After preparing the mold, PDMS mixture was prepared by mixing the base polymer and curing agent at a ratio of 5:1, degassed, and then poured onto the mold. To have a uniform PDMS layer, PDMS was spun on the mold using a two-step coating process to obtain 1 mm thick PDMS. The first layer was coated at 200 rpm for 60 s and cured on a hot plate at 90 °C for 5 min. Then, the second layer was coated at 100 rpm for 60 s and cured at 90 °C for 3 h. Then, PDMS is peeled off. In our design, the microchannel height and width are 200 μm and 50 μm, respectively.

For experimental analysis, particles' position at the outlet was observed using side view imaging. For this purpose, PDMS was cut from 2 mm distance from the channel to see the particle position. To finalize the fabrication of flexible "tape'n roll" devices, we seal the chips using 30 μm-thick Kapton® tape (Figure 2.14b). This tape when sealed to PDMS can tolerate high pressures[62] and can be bent easily. Aluminum posts with different diameters and pitches were prepared by CNC machining, and then the chip was rolled along the grooves on the post (Figure 2.14c). To achieve side view microscopic imaging, the system was placed vertically on a petri dish, and fixed with PDMS curing (Figure 2.14d). Photographs of each step are given in Figure 2.15.

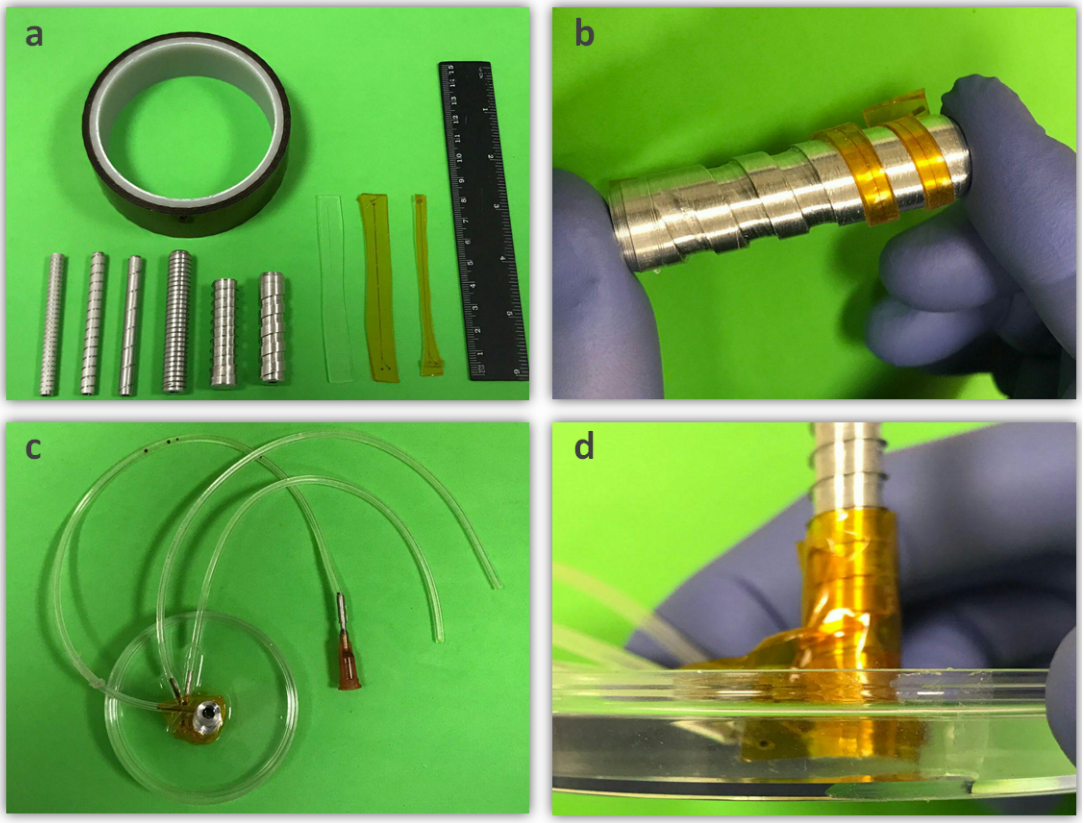

Figure 2.15: Chip preparation steps. a) Representation of all the components used to prepare the chip. b) Thin PDMS layer is rolled over the base to obtain a helical shape. c) The top view and d) the side view of the system fixed on a petri dish by curing PDMS at the bottom for optical observation.

2.4.2 Sample Preparation

We purchased 6 μm diameter polystyrene (PS) microspheres from Polysciences, Inc. and fluorescently labelled them by using hydrophobic pyrene dye. First, 40 mg of pyrene was dissolved in 2 ml of chloroform. 800 μL of 1% SDS solution was prepared in glass vial. Then, 1 ml of the dye-chloroform solution was added to 1% SDS solution. The mixture was sonicated for 5 min in ultrasonic sonicator. 2 ml of PS solution was added to the mixture and covered with an aluminum foil (holes were opened to allow evaporation of chloroform). Then, mixture was put onto hot plate at a temperature of 40 °C and stirred for 24 h in a fume hood. Then, the solution was centrifuged at 4000 rpm for 15 min. At the end, the supernatant was removed and 5 ml of DI water was added and centrifuged again. The last step was repeated twice and finally dye loaded PS beads were dispersed in 5 ml of DI water. Pyrene dye loaded 6 μm polystyrene spheres excited at 340 nm give emission at 470 nm. For red blood cell preparation, blood sample was obtained from an adult donor and collected into blood collection tube with Ethylenediaminetetraacetic acid (EDTA) to prevent coagulation. Then, it was centrifuged at 5000 rpm for 5 min for plasma separation. Afterward, 1 ml of the remained RBCs is mixed gently with 19 ml phosphate buffered saline (PBS) to prepare 20× diluted solution and to prevent cell-cell interaction while they are focusing.

2.5 Experimental Results

2.5.1 Inertial Migration inside 2D Structures

As mentioned above, inertial microfluidics for planar layouts especially spiral design have been studied in detail in the literature. Here, we introduce our novel 2D design called squarel structure to investigate inertial focusing. For both spiral and squarel designs, we analyze red blood cells (RBCs) manipulation and focusing while they are flowing through the microchannel. Spiral structure is

designed in five loops with width, height, and spacing of 350 μm, 50 μm, and 500 μm respectively. As it can be observed from Figure 2.16, by inducing flow rate of 30 ml/h, starting from the first loop, RBCs repel swiftly from the inner wall due to the strong inertial wall lift force and by flowing through the microchannel, RBCs that are far from the inner wall move gently toward the inner wall and finally in the 5th loop, they relax in a narrow region near the inner wall. The focusing of cells in a narrow region results from the balance between inertial lift and Dean drag force due to the curved microchannel. Next, squarel design was analyzed. This design has five loops (width: 450 μm, height:50 μm, spacing, 1 mm) starting from center toward the outer part. As randomly distributed RBCs flow through the microchannel, similar to the spiral design, cells travel across the streamlines to align in a slim region near the inner wall as shown in Figure 2.17. However, in this design there is a slightly different focusing mechanism compared to the spiral structure. Here, the Dean effect is not continuously created through the microchannel length. Instead, in the sharp corner, secondary flow is created. Since, these corners are sharp enough, the discretely created secondary drag force is strong enough and it can balance inertial lift force even in small number of corners. Therefore, by using such an easy planar design, RBCs can be focused and it can be used as a method for plasma extraction from the blood.

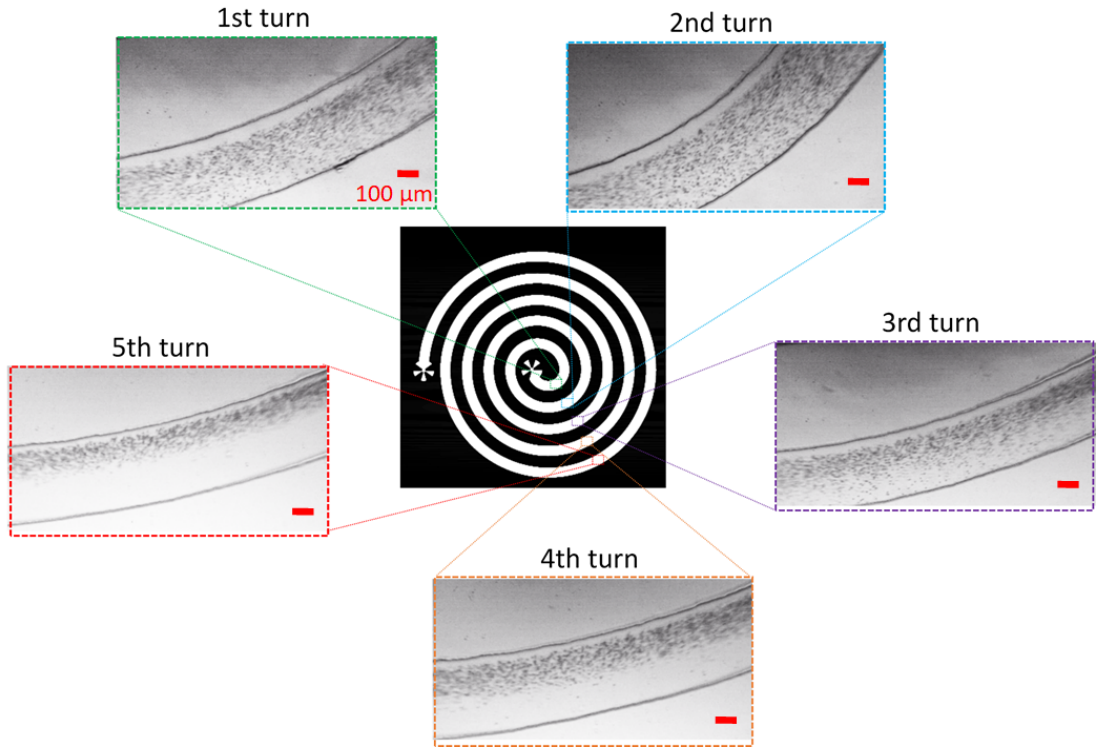

Figure 2.16: RBS focusing inside spiral microchannel. By traveling along the channel, cells start to align in the region near inner wall due to the balance between inertial lift force and Dean drag force. Scale bars are 100 μm

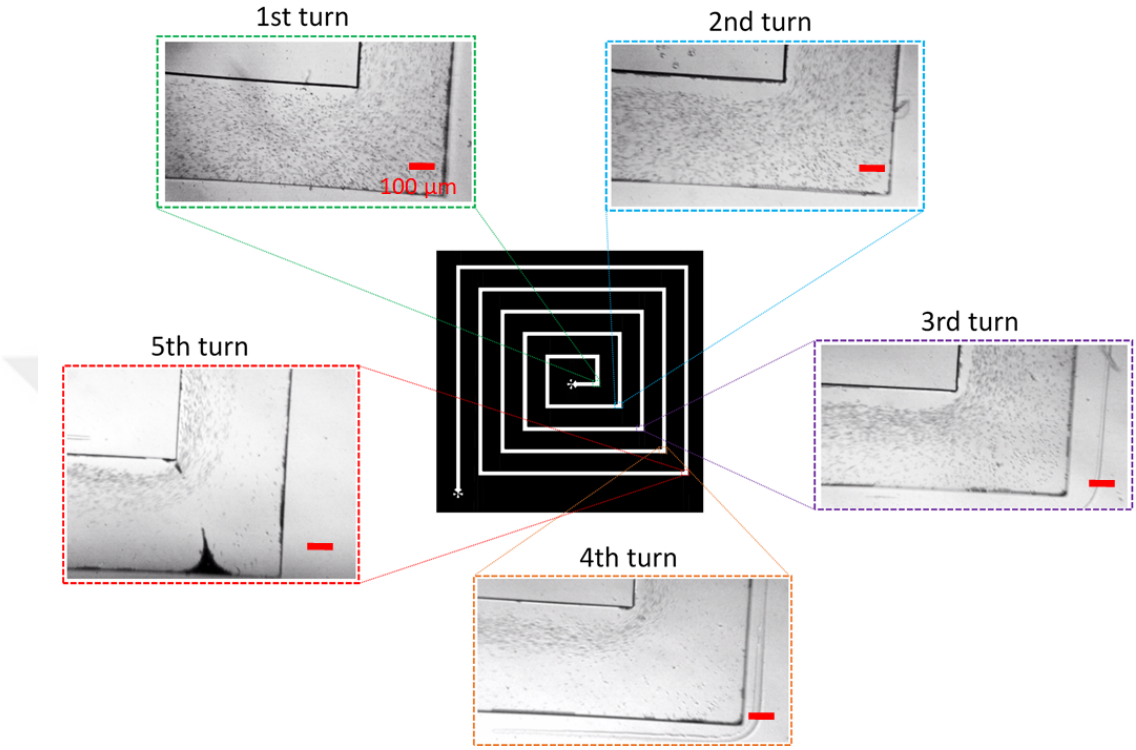

Figure 2.17: RBS focusing inside squarel microchannel. By flowing along the channel, cells start to align in the region near inner wall due to the balance between inertial lift force and Dean drag force. In this case, Dean effect is created in the sharp corners. Scale bars are 100 μm

2.5.2 Inertial Migration inside 3D Helical Microchannels

In the literature, particle migration using inertial focusing for planar spiral structures has been studied in detail. The main contribution of this thesis is the fabrication of 3D helical structures with a novel technique and investigating the inertial particle focusing performance computationally and experimentally. We have studied the effect of 3D helical structure by changing geometrical parameters. As seen from our numerical results given in the previous sections, the optimal focusing results were obtained by using relatively large particles (d>3 μm) and with small rod diameters (4 mm<D<8 mm). Therefore, for the experiments we used 6 μm diameter particles and a rod of 6 mm diameter.

The fabrication of the 3D helical channels is explained in detail in the Materials and Methods section (section 2.4.1). We would like to emphasize that the "tape'n roll" method allows easy modification of the helix pitch. We have prepared two aluminum rods with 6 mm diameter with pitch (P) of 4 mm and 8 mm. We used the same mold to obtain two 8 cm-long PDMS microchannels with an aspect ratio of 4 (W $\times$H=50$\times$200 μm^2). These channels are sealed by Kapton® tape and rolled over the rods to obtain helical channels with different pitches.

Experimental observations were done using the side view imaging setup as shown in Figure 2.14d. Fluorescently tagged spherical polystyrene beads were used to evaluate the migration behavior. Optical microscopy images were obtained at the channel outlet (L=8 cm) using a CMOS camera (OPTIXCAM OCS-5.0). We have varied the flow rate as 10 ml/h, 20 ml/h, and 40 ml/h for two different pitches 4 mm and 8 mm. The microscopy images for different experimental conditions are given in Figure 2.18. To remove the noise due to adherent particles and channel imperfections, background subtraction was performed. Normalized florescence intensity (NFI) of the particles across the channel cross section is given in Figure 2.18.

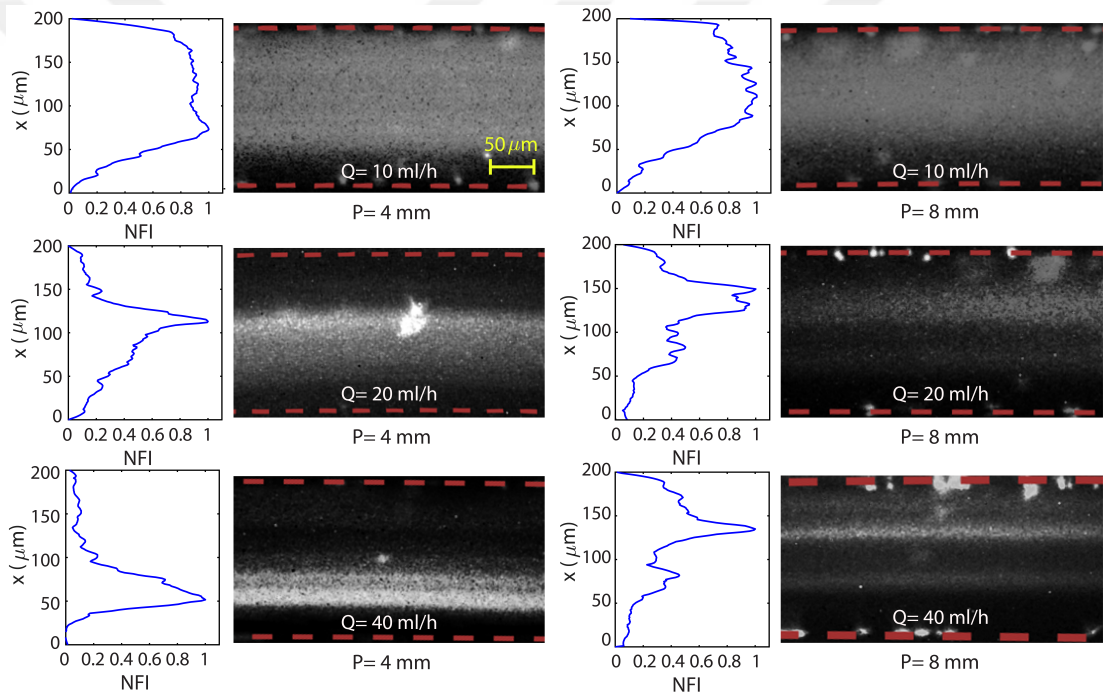

Figure 2.18: Normalized florescence intensity (NFI) together with fluorescence photograph of focusing of 6 μum diameter particles for varying helix pitch length and flow rates. All the images are taken at 100 μm upstream the outlet using the side view imaging method. Background image subtraction was performed to reduce the noise due to the adherent particles and channel imperfections.

For P=4 mm and flow rate 10 ml/h, particles cover roughly the whole microchannel. By increasing the flow rate to 20 ml/h and 40 ml/h, they intend to align near the inner wall. When P=8 mm at low flow rate, particles are wide spread in the microchannel. Increasing the flow rate, results in the formation of two focusing trains near the walls at 40 ml/h. This effect shows the importance of the geometrical parameters and the flow conditions on particle focusing behavior. Beside, by using the 3D helical channels, double train focusing displacement can be observed by simply changing the helix pitch.

Finally, the same microchannel has been configured in spiral and helical forms for a comparison of their focusing behavior (Figure 2.19). For spiral configuration, a 3 mm thick transparent PMMA slab was used as a chip holder for the rolled Kapton tape sealed PDMS chip. The spiral shape structure was opened on the slab using a CO2 laser cutter (Epilog Zing 30 W). The laser operates at 10.6 μm wavelength with 5 kHz frequency and 30 W maximum output power. We used the laser in vector cut mode at maximum frequency and power with 100 μm beam diameter, 1000 DPI resolution, and at 2.6 mm/s speed to cut shadow spiral pattern on PMMA substrate. Shadow grooves on PMMA was designed to match the size of PDMS thickness. We rolled PDMS chip spirally and placed into the PMMA structure (Figure 2.19a). The inner starting and outer ending radius of the spiral was chosen as 4 mm and 10 mm, respectively, which can be tuned very easily.

For the helix configuration, 6 mm helix diameter and 4 mm pitch rod was used. The sealed PDMS chip was rolled onto the grooves of the rod (Figure 2.19b). The two configurations were compared for their RBC focusing performance.

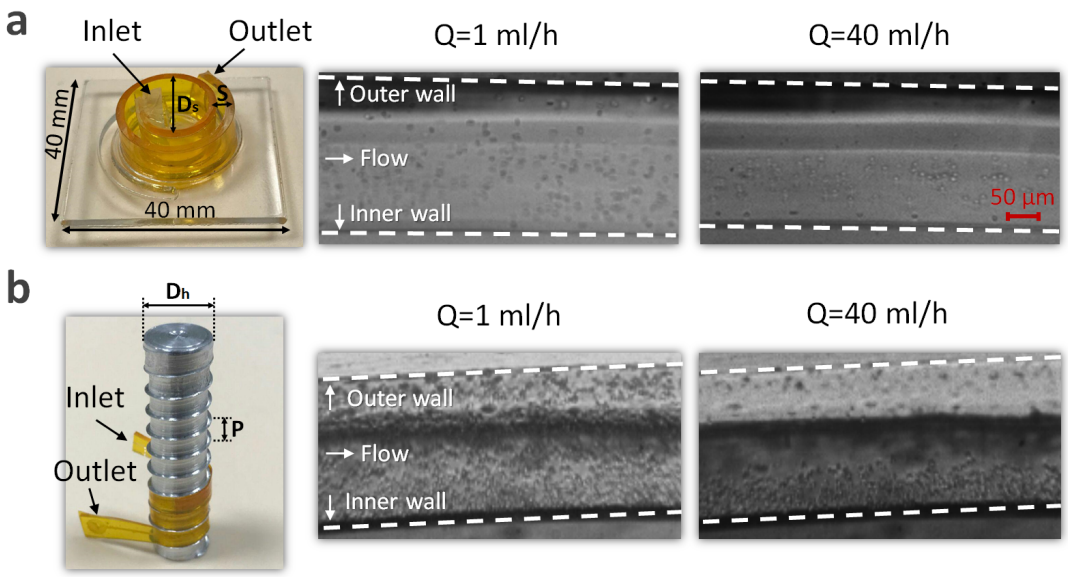

Figure 2.19: Focusing of red blood cells for two different curved structures. a) For the spiral structure with starting radius, end radius and spacing of 4 mm, 10 mm, and 4 mm, respectively. For 1 ml/h flow rate cells are distributed inside the channel. Increasing the flow rate to 40 ml/h leads to focusing of cells in half of the channel near the inner wall. b) For helical structure with diameter and pitch of 6 mm and 4 mm, respectively, increasing the flow rate from 1 ml/h to 40 ml/h leads to focusing near the channel inner wall.

Figure 2.19 shows the side-view microscope images of the cells at the closest point to the outlets for two different flow rates of 1 ml/h and 40 ml/h. For both cases, at low flow rate (1 ml/h) RBCs are dispersed across the microchannel. Increasing the flow rate to 40 ml/h leads to the confinement of the cells near the inner wall covering nearly half of the channel. For spiral configuration, spacing between spiral turns was chosen large enough (4 mm). To confine focused RBCs in a narrower region closer to the inner wall, spacing should be chosen as small as possible and/or length of the channel should be designed large enough. For the helical configuration, helix pitch is a critical parameter. If the aim is to focus particles or cells in a narrow region, helix pitch should be chosen as small as possible. For the two geometries compared here, a similar focusing performance was obtained.

2.6 Conclusion

In this chapter, inertial migration of particles inside 3D helical microchannel is investigated through computational modeling and experimental approach. Later, inertial migration of RBCs in 2D structures (spiral and squarel) has been investigated experimentally. To obtain a helical microchannel, a novel "tape'n roll" method is introduced. The effects of helix diameter, pitch, aspect ratio of channel, particle size, and flow rate on particle migration are explored at low particle concentration case. It is shown that particles have helical motion along the channel and by tailoring the effective parameters, various migration behaviors can be observed. The main difference of this 3D structure from planar spiral geometry is the asymmetry of the Dean vortices which can alter particles' equilibrium position. For sufficiently high pitches, particles can focus in the diagonal of the rectangle channel cross section. Some of the key points obtained from these results are summarized below:

1- Particles are affected by different lift and Dean drag forces depending on their position across the channel. Therefore, for large particles ($a/D_h > 0.07$), length of the channel should be chosen long enough to guarantee the alignment

of particles in focusing stream(s).

2- For 3D helical design the radius of curvature is kept constant, however, helix pitch distorts the symmetry of the Dean vortices. Increasing the helix pitch skews the position of the two attractor points. Therefore, to avoid diagonal focusing of the particles, helix pitch should be as small as possible.

3- The tape'n roll fabrication method, allows one to easily modify the channel structure while maintaining the channel cross section and the length. Additionally, in case of any clogging or contamination, the sealing tape can be removed and the structures can be cleaned and reconstructed in minutes.

Chapter 3

Migration of Particles inside Viscoelastic Fluids

To date, several microfluidic techniques have been developed to achieve 3D focusing of particles. Sheath flow supported hydrodynamic focusing[63, 64, 65, 66, 67] requires squeezing of the suspension fluid with sheath fluid in order to create a narrow, size-adjustable width of sample flow in microfluidic channel. Such systems suffer from the use of extensive amount of sheath fluid, require precise fabrication, and high accuracy on flow control. In addition to hydrodynamic focusing, electric[11, 68], magnetic[13] or acoustic forces[14, 69] can be used to focus the particles along the same line, which we refer as 3D focusing (in some studies, called as 2D focusing due to focusing forces along both lateral dimensions[70, 71]). These methods require additional actuation forces to induce particle focusing and increase the fabrication and operation complexity.

On the other hand, inertial[72, 19, 18, 73] and viscoelastic focusing[5, 4, 16, 74, 75, 76, 77] techniques allow sheathless single inlet/outlet chips, which provides simplicity in fabrication and operation. Both techniques are highly dependent on fluid properties and flow regime. As discussed in the previous chapter, for Newtonian fluids, inertial lift force causes the particles to migrate across the velocity streamlines due to velocity gradient across channel cross section. When

inertial forces are dominant compared to viscous forces, particles move to equilibrium positions inside medium. Inertial focusing has been investigated for straight channels of different geometries including circular[78], square[38], rectangular[39] and even unusual cross sections[40] resulting in multiple-line focusing. Implementing curved structures, Dean drag force is created to focus particles into a narrower region[19, 79]. However, to reach single-train of particles, structure of the channel should be engineered or different structures of channels should be integrated in a specific sequence.

Recently, non-Newtonian viscoelastic fluids have attracted great attention[80, 81, 82, 83, 84, 85] as an alternative to inertial focusing. Inertial focusing is implemented by optimizing the channel dimensions, channel geometry, and flow rate for a specific particle size. Viscoelastic focusing provides an additional degree of freedom which is the ability to tune the rheological properties of the carrier fluid. Viscoelastic fluids are prepared by adding biological[86, 87] or synthetic polymeric powders[88] to Newtonian solvents so that the solution shows viscoelastic behavior, and thus elastic force is exerted to the suspended particles.

In this chapter, we analyze and characterize particles by combining optical microscopy and viscoelastic particle focusing technique as schematically shown in Figure 3.1. Three non-Newtonian fluids have been evaluated for achieving high performance 3D particle focusing. Then, the optical detection was done by using a high speed camera mounted on optical microscope to track indivudual particles by recording video. Then, the video is converted to image frames and by image processing, particles size and position at the outlet are extracted. The system does not require any microfabrication steps and can be assembled on a finger-sized substrate. Finally, our results show that hyaluronic acid (HA) and polyethylene oxide (PEO) with specific molecular weight can be used to focus 6 μm diameter particles to the center of the capillary at high accuracy, introducing a new technique for flow cytometry purpose.

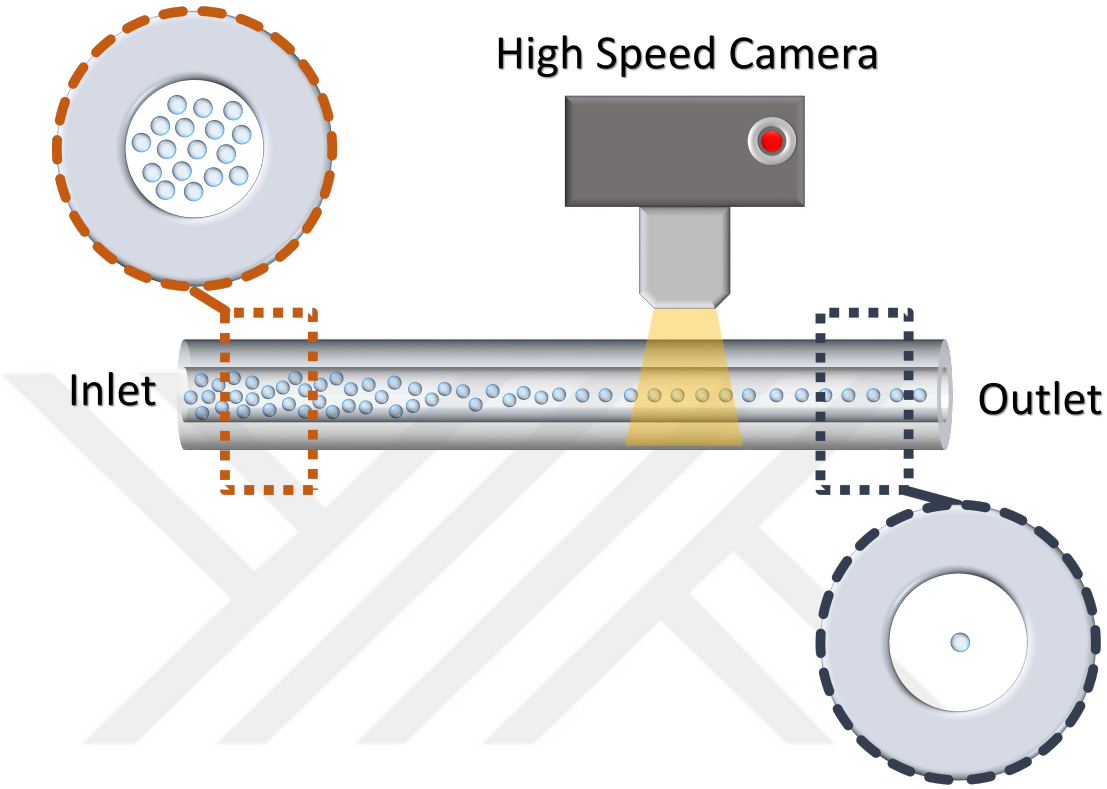

Figure 3.1: Schematic illustration of sheathless focusing chip and detection setup consisting of a simple circular capillary tube and the high speed camera for imaging. Particles are focused at the center of circular capillary channel due to viscoelastic forces. 6 cm away from the inlet, bright-field image of the particles were recorded and analyzed in MATLAB to find the position of particles.

3.1 Theory

Elastic behavior of viscoelastic fluid originates from the suspension of polymers inside solution. This non-Newtonian behavior induces elastic force due to normal stress differences[89]. Under non-Newtonian Poiseuille pipe-flow, two normal stress differences can be defined as

$$N_1 = \sigma_{zz} - \sigma_{rr} \tag{3.1}$$

$$N_2 = \sigma_{rr} - \sigma_{\theta\theta} \tag{3.2}$$

where z, r, and θ denote flow, radial, and vorticity directions, respectively. Diluted, constant shear viscosity solutions are considered to be Boger fluids[90] and can be studied by Oldroyd-B model. For Boger fluids, the second normal stress difference (N_2) is negligible compared to the first normal stress difference (N_1). Therefore, elastic force (F_e) can be written as[3]

$$F_e \approx a^3 \frac{\partial N_1}{\partial r} \tag{3.3}$$

To characterize elasticity, Weissenberg number is defined as

$$Wi = \lambda \dot{\gamma} \tag{3.4}$$

where is λ relaxation time and $\dot{\gamma}$ is shear rate. To compare elasticity and inertia, elastic number is defined as

$$El = \frac{Wi}{Re} \tag{3.5}$$

In pipe flow, radial migration velocity for a particle under the effect of elastic force is given as[91]

$$V_r \propto a^2 Wi \frac{\partial \dot{\gamma}}{\partial r} \tag{3.6}$$

To relate the radial migration velocity to geometrical parameters and solution properties, equation (3.6) can be written as[92]

$$V_r \propto \frac{0.77 \frac{c}{c^\star}}{1 + 0.77 \frac{c}{c^\star}} Wi (\frac{a}{R})^2 \frac{r}{R} \tag{3.7}$$

where c, c*, a, R and r are polymeric concentration, overlapping polymer

concentration, particle radius, channel radius and radial position of particle, respectively. In the analytical results section, by using the above equations, focusing performance of the particles inside PVP_{40kDa}, PEO_{5MDa}, and $HA_{1.06MDa}$ is analyzed through analytical approach.

3.2 Materials and Methods

3.2.1 Sample Preparation

3D focusing using viscoelastic force is highly dependent on the rheological properties of the viscoelastic fluid. Therefore, it is critical to evaluate the performance of the image cytometer using different fluids. For this study, we have investigated three different biocompatible polymers to prepare viscoelastic fluids: polyethlyene oxide (PEO, M_w=5×10^6 Da, Sigma-Aldrich), polyvinylpyrrolidone (PVP, M_w=4×10^4 Da, Sigma-Aldrich) and hyaluronic acid (HA, M_w=1.06×10^6 Da, Binisu Schimoto). PEO, PVP, and HA were dissolved in DI water at 0.05% (w/v), 8% (w/v), and 0.5% (w/v) concentrations, respectively. We characterized the rheological properties of the viscoelastic fluids using a rheometer (Anton Paar, MCR 301). Figure 3.2 shows the viscosity of the fluids as a function of shear rate. PEO and PVP show nearly constant viscosity, especially in the shear rate range observed during our experiments ($\dot{\gamma}$<2000 s^{-1}). However, HA shows a shear thinning behavior. For the experiments, 6 μm diameter polystyrene microbeads (Polysciences, Inc.) were suspended in the viscoelastic solutions at a concentration of 4×10^6 particles/ml. The samples were continuously mixed to have uniform particle concentration throughout the experiments.

3.2.2 Experimental Setup and Data Processing

Glass capillary tube with inner diameter (ID) of 60 μm and outer diameter (OD) of 190 μm was purchased from Polymicro Technologies. To achieve fluidic access

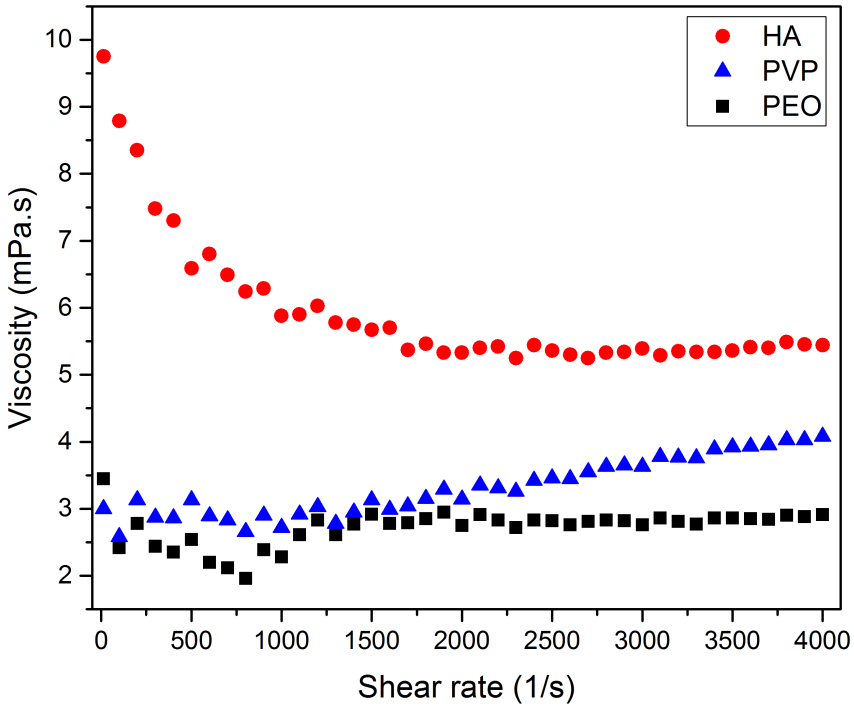

Figure 3.2: Viscosity of the fluids as a function of shear rate for three different viscoelastic solutions: 0.05% (w/v) PEO, 8% (w/v) PVP, and 0.5% (w/v) HA in water.

to the capillary, the capillary was inserted into a PDMS channel at the inlet. A pressure pump was used (Elveflow, OB1 2 bar) to deliver the polystyrene microsphere suspended viscoelastic fluids to capillary tube. The manipulation of the particles and their distribution inside the capillary tube were observed under an inverted microscope (Omano, OMFL600) attached to a high-speed camera (Vision Research, Phantom Miro M310). Figure 3.1 shows the schematic of all the components of the measurement device. Particle position and distribution along the capillary tube were recorded with the high-speed camera and post-processed with MATLAB. To extract image stack, first of all, video is converted to image frames in sequence in grayscale. Then, each image is subtracted from background. To process border pixels in the substracted images, erosion and dilation were applied. These steps allow to assign maximum (255) and then minimum (0)

values for the subtracted images to create a clear dark field images. Finally, images are combined to reveal the trace of particles. This method is inspired by the technique used by Amar Basu for droplet morphometry and velocimetry (DMV) analysis[93].

3.3 Analytical Results

Viscoelastic focusing is highly dependent on the rheological properties of the fluids. According to equation (3.7), particle migration velocity (V_r) is a function of polymeric concentration (c), overlapping polymer concentration (c*), and relaxation time (λ) for a given combination of shear rate ($\dot{\gamma}$), blockage ratio (a/R) and radial position (r/R). A rheological term can be defined as $\frac{0.77\frac{c}{c^\star}}{1+0.77\frac{c}{c^\star}}\lambda$ that reflects the influence of the viscoelastic fluid on particle migration velocity. Relaxation time for polymers was estimated using the Zimm relaxation time $\lambda{\sim}4\pi\eta_s R_g^3 k_B$T where k_B,T, η_s, and R_g correspond to Boltzmann constant, temperature, solvent viscosity, and radius of gyration of polymer[94], respectively. R_g for PEO_{5MDa}[95], $HA_{1.06MDa}$[96], PVP_{40kDa}[97] were found from the literature. c* values were determined by using Graessley's modified equation[98] where c*=$0.77/[\eta]$. $[\eta]$ is the intrinsic viscosity, depends on polymer type and its molecular weight.$[\eta]_{PEO}$, $[\eta]_{PVP}$, and $[\eta]_{HA}$ were found from the literature[96, 99, 100] as $7.2{\times}10^{-2}(M_w)^{0.65}{\approx}1628$ ml/g, $3.93{\times}10^{-2}(M_w)^{0.59}{\approx}20.4$ ml/g, and $3.21{\times}10^{-2}(M_w)^{0.783}{\approx}1676$ ml/g respectively. The calculation of the rheological term is given in Table 3.1 for PEO, PVP, and HA. As seen from this analysis, PEO and HA yielded higher $\frac{0.77\frac{c}{c^\star}}{1+0.77\frac{c}{c^\star}}\lambda$ and similar values, thus leading to faster focusing of the particles. Next, numerical simulation is used to compare the focusing efficiency.

Table 3.1: Calculation of the rheological term used for particle velocity analysis.

Fluid	R_g (nm)	c (g/ml)	$[\eta]$ (ml/g)	$c^\star$ (g/ml)	λ (ms)	$\frac{0.77\frac{c}{c^\star}}{1+0.77\frac{c}{c^\star}}\lambda$ (ms)
PEO	155.4	0.0005	1628	0.000473	11.39	5.11
PVP	14.4	0.08	20.40	0.037747	$9.06{\times}10^{-3}$	$5.62{\times}10^{-3}$
HA	126.1	0.005	1676	0.000459	6.08	5.43

3.4 Numerical Simulation

We performed numerical simulations with COMSOL 5.2 to analyze the focusing effect of three viscoelastic fluids that have different relaxation times and viscosities. Since elastic force is mainly affected by N_1, N_2 is not considered in the simulations. Oldroyd-B model was used to define the stress due to the elastic effect. Navier-Stokes, continuity, and additional stress contribution in non-dimensional form are defined as

$$Re(u.\bigtriangledown)u = \bigtriangledown.\big[-pI + \mu_s\big[\bigtriangledown u + (\bigtriangledown u)^T\big] + T\big] \tag{3.8}$$

$$\bigtriangledown.(u) = 0 \tag{3.9}$$

$$T + Wi((u.\bigtriangledown)T - \big[(\bigtriangledown u)T + T(\bigtriangledown u)^T\big]) = \mu_p(\bigtriangledown u + (\bigtriangledown u)^T) \tag{3.10}$$

where Re, T,μ_s,μ_p, and u correspond to Reynolds number, additional stress tensor, relative viscosity of solvent and polymer, respectively. The relation between relative viscosities is

$$\mu_p = \frac{\eta_p}{\eta} = 1 - \mu_s \tag{3.11}$$

Based on our results given in Figure 3.2, relative solvent viscosities of PEO and PVP solutions (μ_s) were taken as 0.357 and 0.333. On the other hand, HA behaves as a shear-thinning fluid, which is implemented using Carreau model as

$$\mu = \mu_{inf} + (\mu_0 - \mu_{inf})\big[1 + (\lambda\dot{\gamma})^2\big]^{\frac{n-1}{2}} \tag{3.12}$$

The above equation was applied to our rheological measurement data shown in Figure 3.2 for HA. Using curve fitting, the Carreau model variables were found

as $\mu_{0,s}$=0.11, $\mu_{inf,s}$=0.2 , λ=3.72 ms, and n=0. By solving equations (3.8), (3.9) and (3.10) together, velocity field and normal stresses were obtained. Later, the first normal stress difference (N_1) was found by subtracting σ_{rr} from σ_{zz} (equation (3.1)). Reynolds number was chosen as 0.01 to neglect inertia effect. Weissenberg numbers for PEO, PVP, and HA were calculated as 0.169, 0.000144, and 0.251, respectively. Using particle tracing module in COMSOL, radial position of the particles along the microchannel was obtained, which allowed us to study the focusing performance.

3.5 Numerical Results

Elastic force acting on suspended particles in the medium is dependent on particle size and first normal stress difference gradient (equation (3.3)). First, we studied the focusing performance of three viscoelastic solutions using numerical simulations. Lateral velocity depends on shear rate gradient as shown in equation (3.6). Under viscoelastic Poiseuille pipe-flow, shear rate decreases from wall to center of the pipe as shown in Figure 3.3a. In our study, we tested 6 μm diameter particles suspended in three different viscoelastic media. N_1 was numerically calculated for these fluids, and the results are given in Figure 3.3b. HA has the highest N_1 gradient whereas PVP has the lowest value. This result suggests that particles in HA solution can be focused faster due to higher elastic force.

Radial migration of particles was analyzed using particle tracing module. Elastic force (equation (3.3)) and drag force (F_d=$6\pi\mu$au) were defined using N_1 and relative velocity (u), which were obtained from laminar flow simulation. Neutral buoyancy was assumed by taking the density of the solutions and the particles the same (ρ=1050 kg/m^3). Particle-particle interactions were not considered. 20 particles suspended in the medium were traced during the simulations.

Figure 3.3c shows cross-sectional position of particles at increasing distances from the inlet (L: axial distance from inlet, D: channel diameter). Particles suspended in PEO and HA solutions were focused at the centerline while PVP

showed dramatically lower performance. These results are in good agreement with the analytical results.

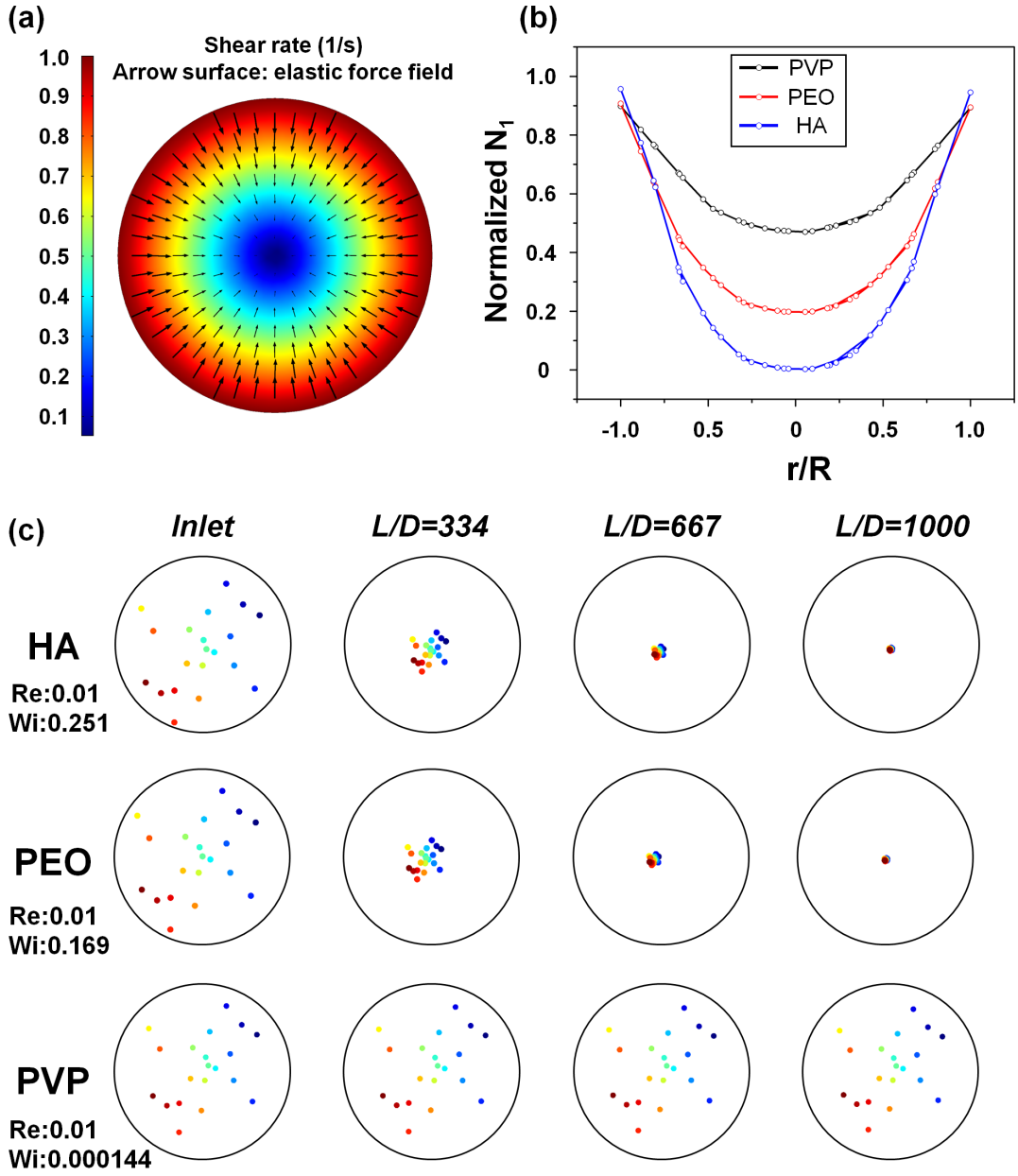

Figure 3.3: Numerical results of viscoelastic focusing: (a) Normalized shear rate for viscoelastic fluid inside cylindrical capillary tube and corresponding elastic force field. (b) Normalized first normal stress difference versus dimensionless radial position, r/R for PVP, PEO, and HA. (c) Cross-sectional position of 20 particles along the capillary microchannel, with 2 cm intervals from the inlet. Here, L and D represent the axial distance from inlet and channel diameter, respectively.

3.6 Experimental Results

3.6.1 Experimental Results on Particle Focusing

The analytical and numerical results demonstrate the effect of the rheological properties of the fluids on the focusing performance. In this section, we analyze the experimental particle focusing performance for all three viscoelastic fluids using the setup explained in the Materials and Methods section (section 3.2.2). The inlet pressure was adjusted so that $Re < 1$ and therefore inertial effect was neglected. To analyze the performance of focusing, motion of particles have been recorded by using the high-speed camera and $\times 10$ objective of microscope Afterward, by image stacking for duration of 0.2 second, position of particles has been extracted and demostrated in a single frame. Moreover, we calculated the probability distribution function (PDF) for each measurement. Calculations were performed from the movies recorded at a distance of 6 cm from the capillary inlet.

Figure 3.4, 3.5, and 3.6 represent image stack of the particles flowing in different flow conditions inside HA, PEO, and PVP solutions respectively. For HA solution, particles are dispersed in low flow rate (Re:0.001, Wi:0.025). By increasing flow rate, they align in a single train in the center-line and success in focusing under the inertial regime (Figure 3.4). The particles inside PEO solution, start to focus when Re>0.181 (Figure 3.5). As shown in Figure 3.6, PVP solution fails to focus particles in a narrow region even by increasing the flow rate (Re:0.236, Wi:0.003). This non-focusing behavior could be due to the minor elastic effect inside the fluid.

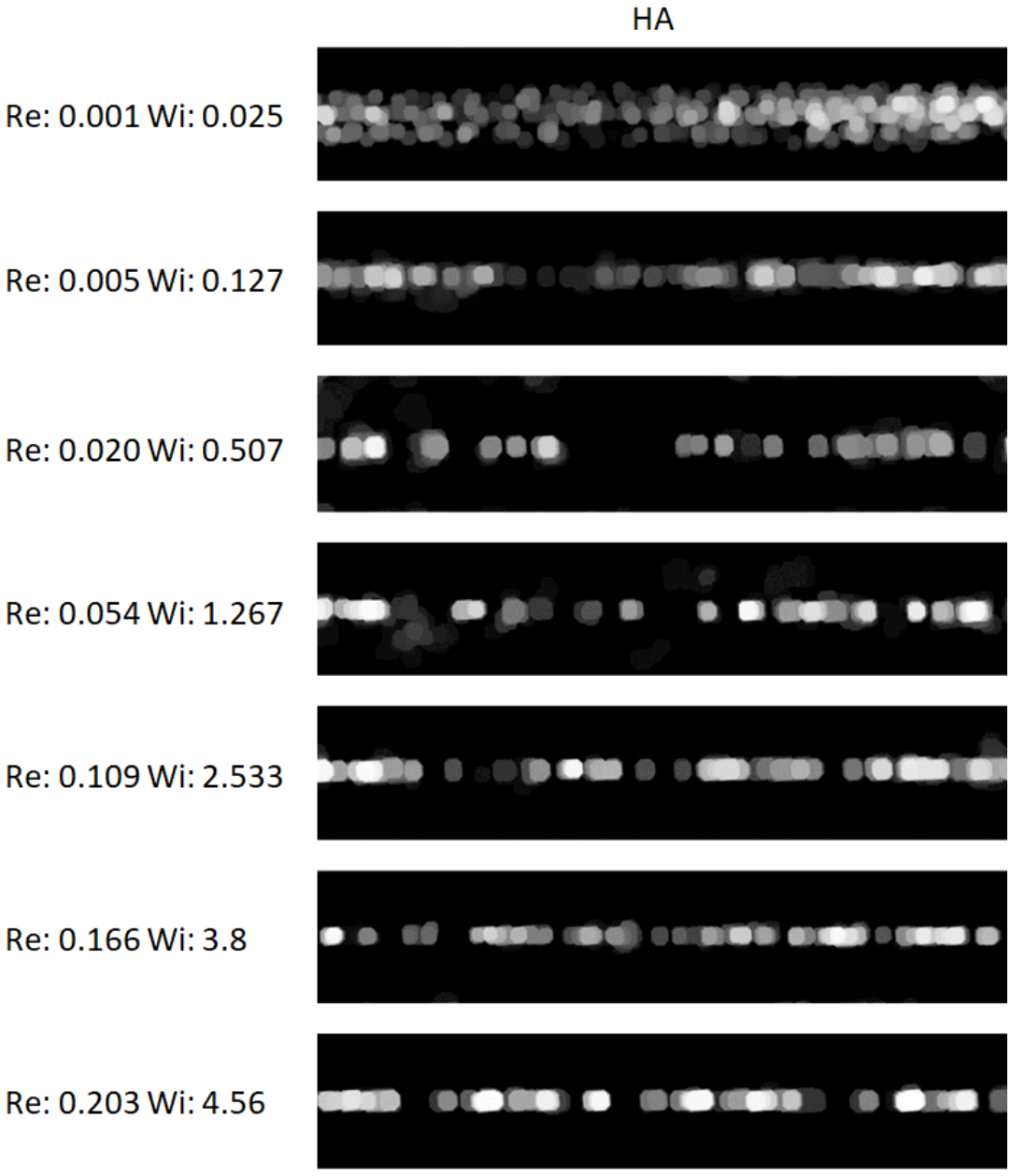

Figure 3.4: Image stack of the particles traveling inside HA solution. By increasing flow rate, particles align at the center of the microchannel.

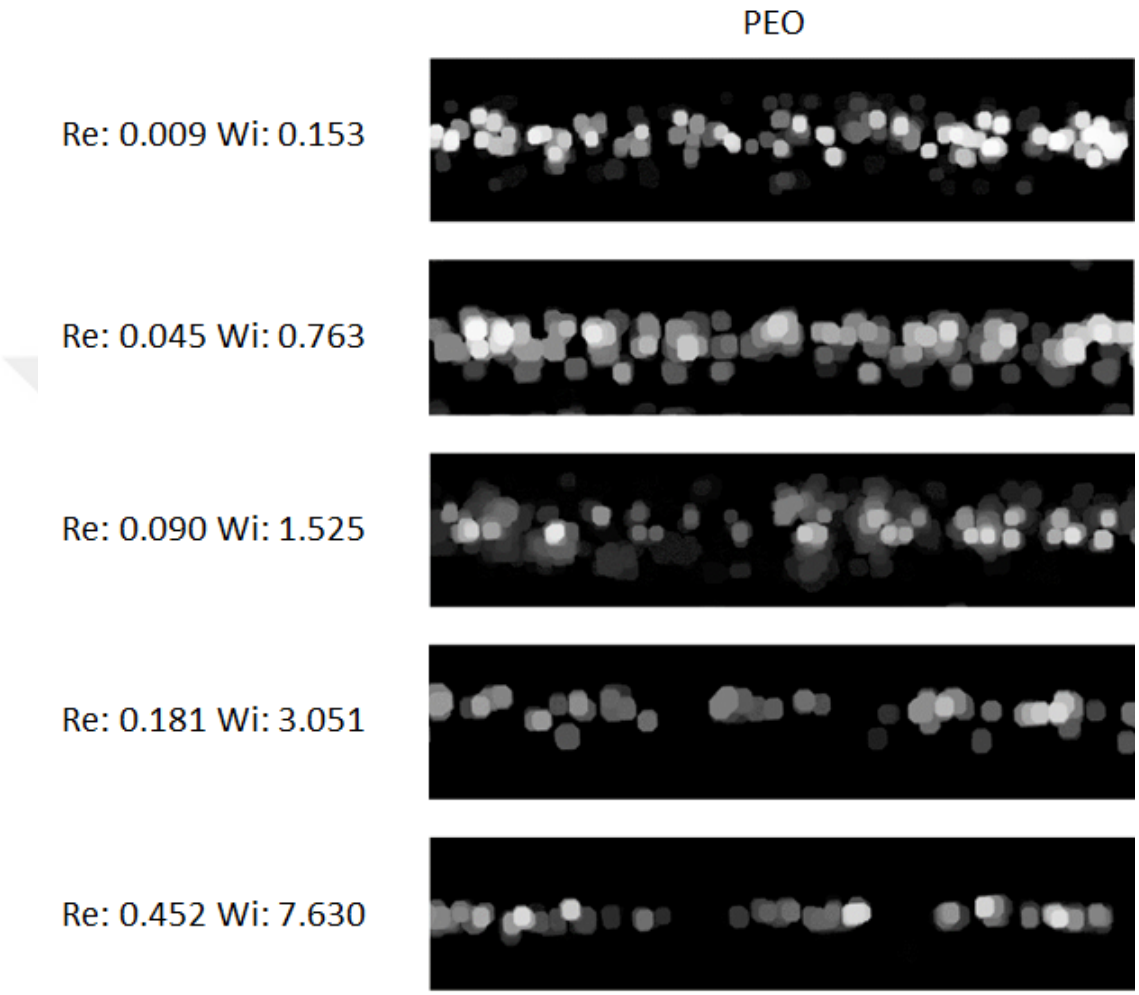

Figure 3.5: Image stack of the particles flowing inside PEO solution. In low flow rates (Re<0.181), particles are distributed inside the microchannel. After sufficiently increasing flow rate (Re>0.181) particles start to focus at center-line.

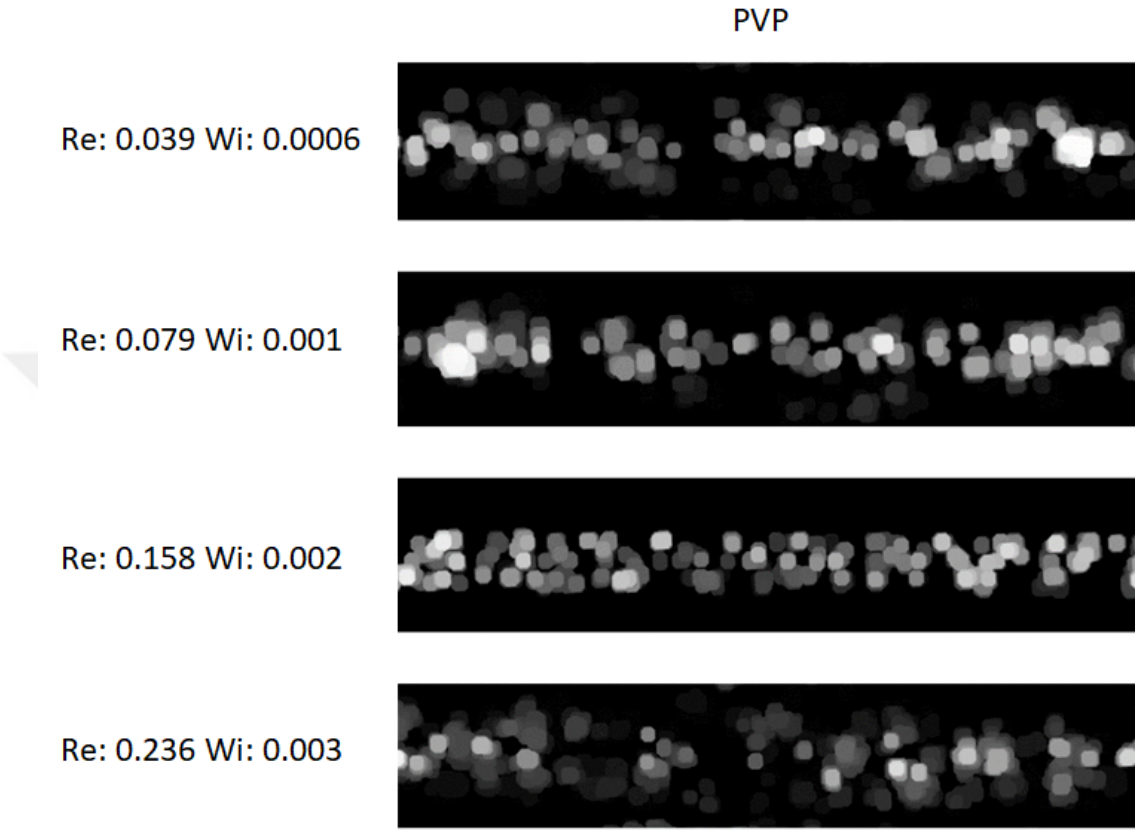

Figure 3.6: Image stack of the particles moving inside PVP solution. Increasing flow rate does not improve the focusing of the particles. PVP solution fails to align particles.

To analyze particle focusing efficient quantitatively, PDF are calculated for each case. Figure 3.7a shows the focusing performance of PVP in the range of $0.039<Re<0.24$, $0.00055<Wi<0.0034$, and $El=0.014$. Partial 3D focusing was observed with wide exponential tails in radial direction. Increasing the pressure does not provide any noticeable improvement, which can be explained with low elastic force on particles and thus low radial velocity. Figure 3.7b shows the PDF results for PEO in the range of $0.009<Re<0.45$, $0.152<Wi<7.593$, and $El=16.874$. Successful 3D focusing was achieved when inlet pressure was increased from 200 mbar to 500 mbar. In Figure 3.7c, PDF results for HA are given in the range of $0.00088<Re<0.2$, $0.025<Wi<4.56$, and $22.8<El<28.41$. Here, we observed better 3D focusing performance compared to PEO and PVP even at low flow rates. Furthermore, the focusing efficiency is almost the same for inlet pressure values beyond 200 mbar. This provides a wide inlet pressure adjustment range, which is critical to obtain the highest throughput.

3.6.2 Experimental Results on Cytometry

Both analytical calculations and experimental PDF values demonstrate that the viscoelastic focusing is ideal for sheathless flow cytometry purpose. Afterwards, we performed position and size measurements with the image microflow cytometry technique to compare the performance of three different viscoelastic fluids. The pressure values for HA, PEO, and PVP were set to 1000 mbar ($Re=0.11$), 500 mbar ($Re=0.45$), and 300 mbar ($Re=0.24$), respectively.

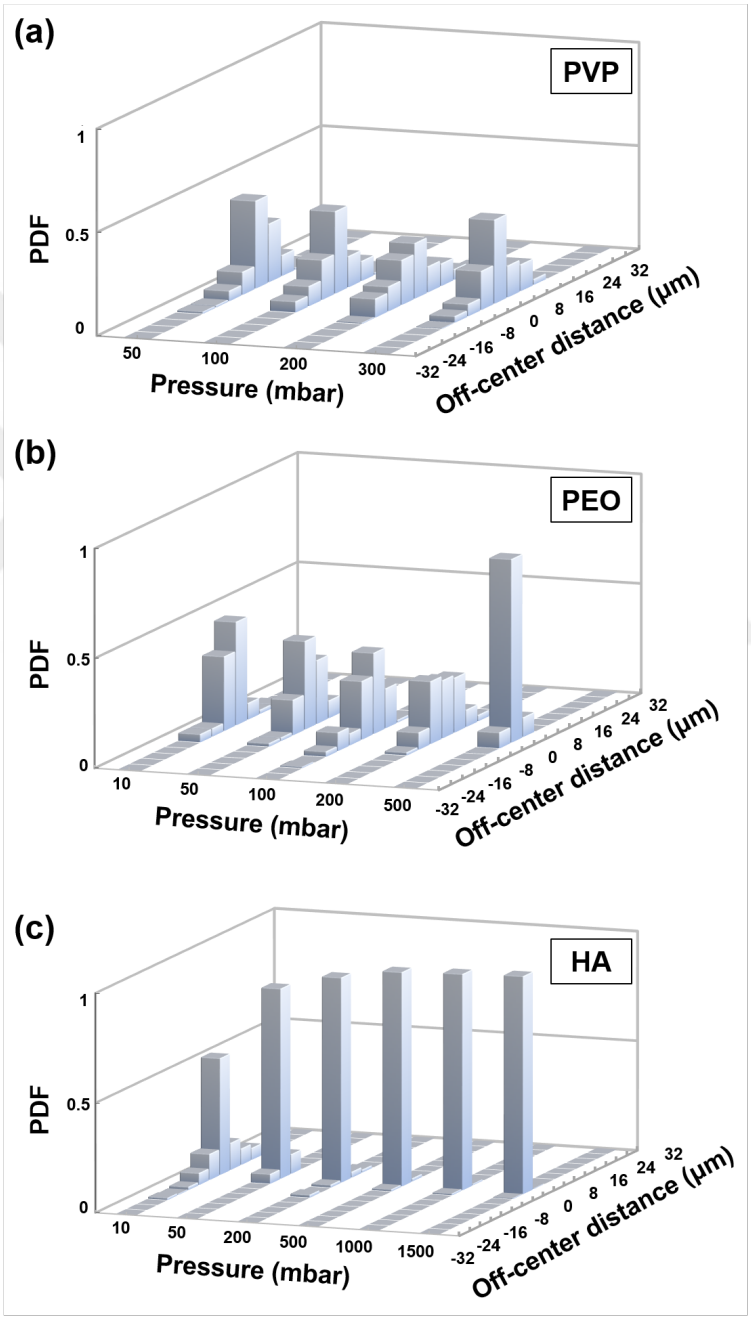

Figure 3.7: Probability distribution function (PDF) of particle distribution across the cylindrical capillary microchannel width (inner diameter 60 μm) as a function of inlet pressure: (a) PVP, (b) PEO, and (c) HA solutions.

Figure 3.8 represents scatter plot of size vs radial position of 672 particles as well as histograms for size and radial position for HA solution. In closer look-up to scatter plot, we observe that particles are accumulated in narrow region in the centerline with misalignment of 1 μm. This yields to standard deviation of 0.133 and mean value of 29.26. For size analysis, particles are distributed from 6 μm to 8 μm. This distribution can be resulted from aggregation of the particles resulting in extended boundaries for particles and larger size detection in the region of analysis.

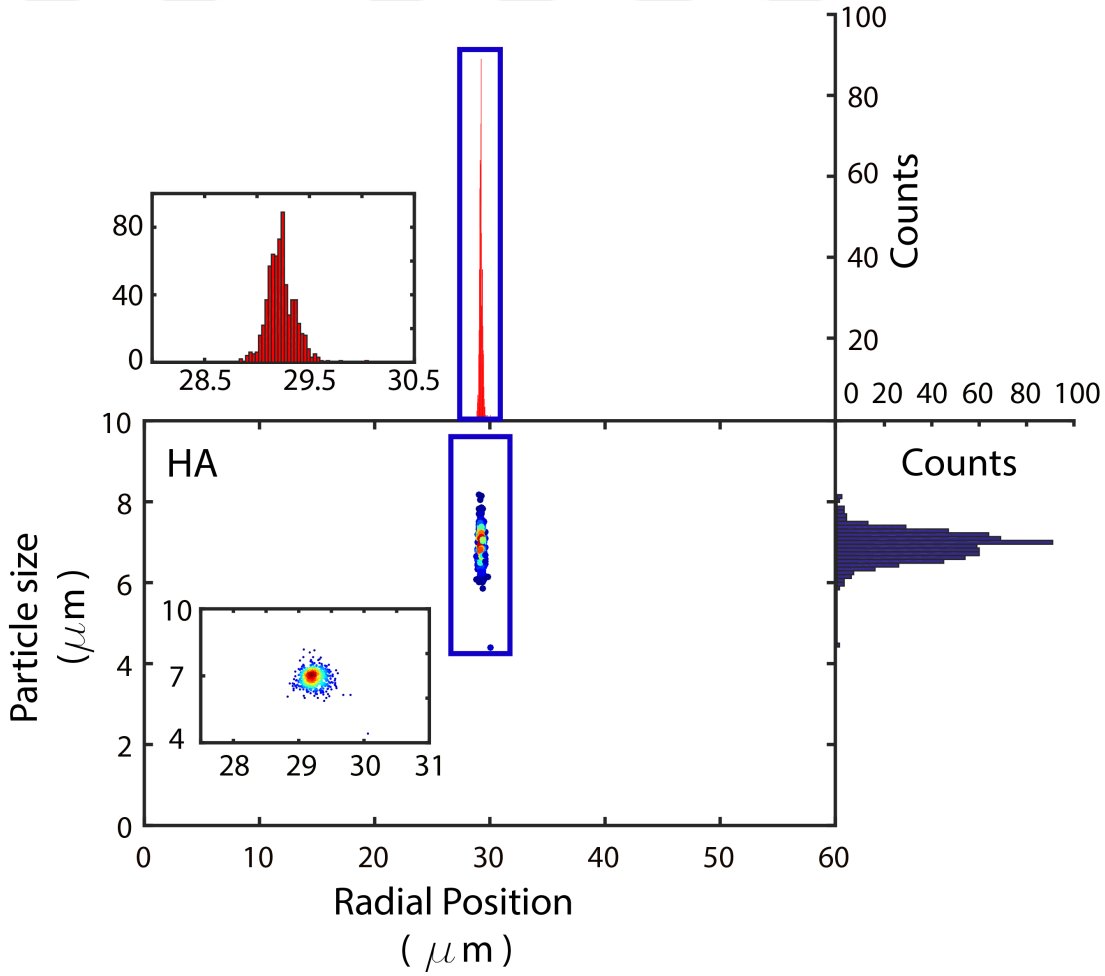

Figure 3.8: Scatter plot of particle size vs. radial position together with histograms of size and position for HA solution. Due to the perfect alignment of the particles in center-line (1 μm width), histogram of position and scatter plot are shown in close look-up.

Figure 3.9 represents histogram and scatter plot of particle size vs radial position resulted from 836 events for PEO solution. In this case, particles have wider distribution compared to HA solution. Similar to the previous case, size distribution might be resulted from doublets and failure in perfect detection of the boundary for particles. The standard deviation and mean values of 1.745 and 29.26 were obtained for radial position of particles, respectively.

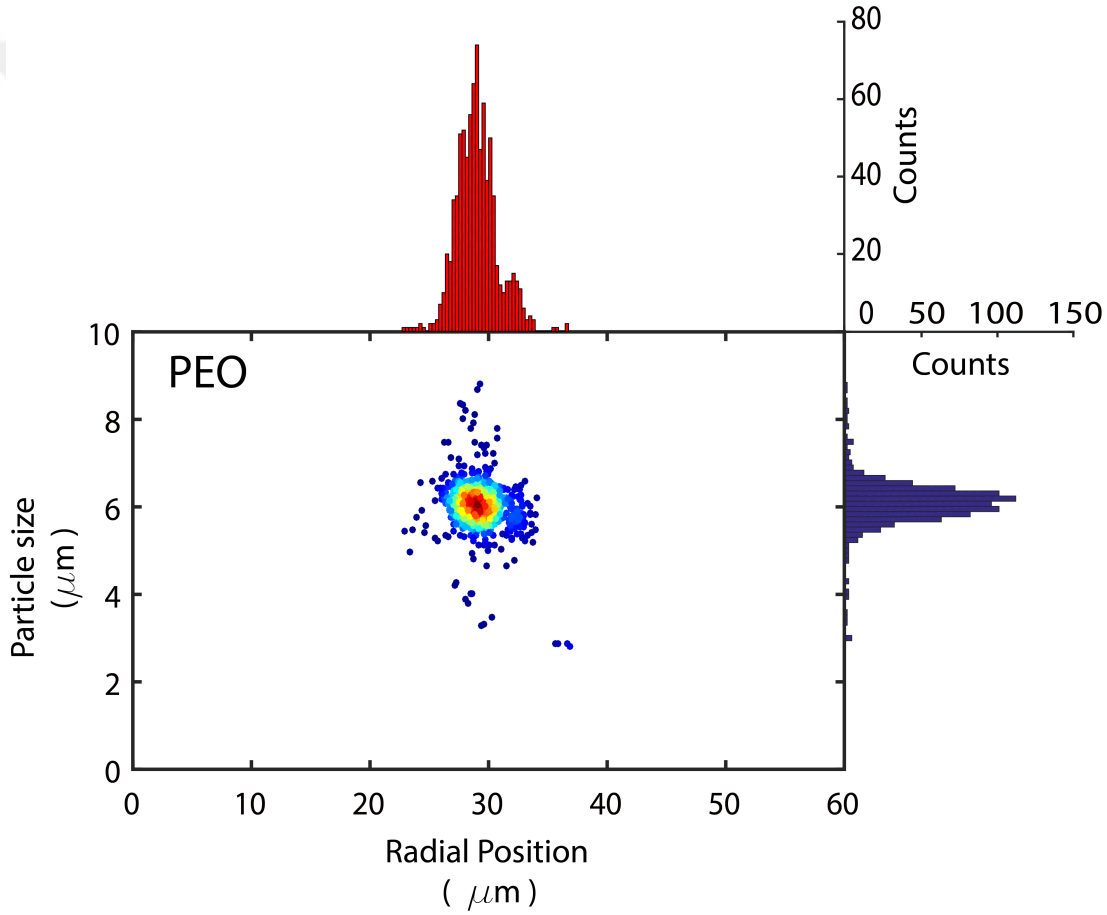

Figure 3.9: PEO based scatter plot of particle size vs. radial position together with histograms of size and position.

For PVP solution, 1503 particles were tracked. In Figure 3.10, scatter plot of size vs radial position has two accumulated regions. Weak 3D focusing performance of PVP causes fleeing particles. Detected beads show large radial position variation and disrupted periodicity. The standard deviation and mean values for PVP were obtained as 4.389 and 29.24, respectively. Compared to the results obtained using PEO and HA solutions that are densely populated in a narrow region, PVP events are dispersed. Therefore, we conclude that PVP (M_w= 4104 Da) is unsuccessful for flow cytometry.

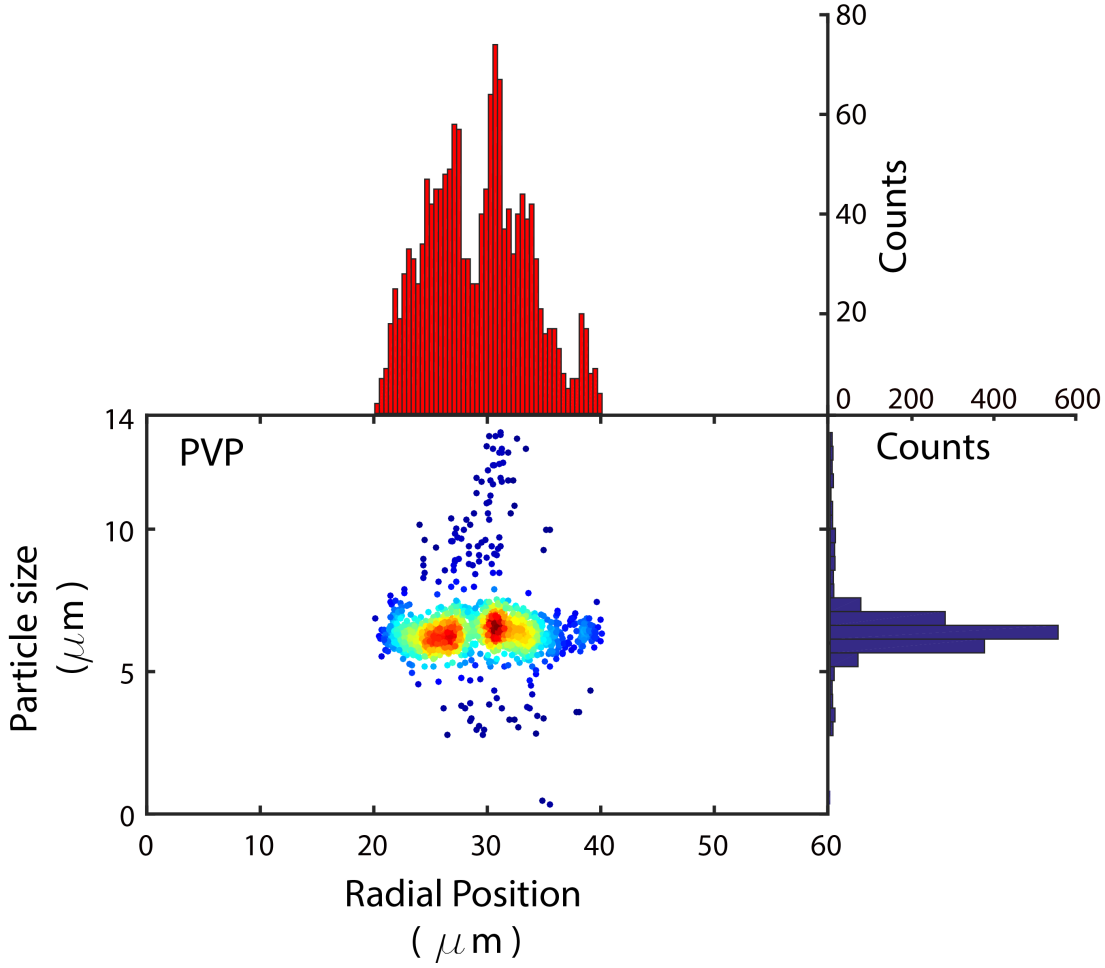

Figure 3.10: Scatter plot of particle size vs. radial position together with histograms of size and position for PVP solution. Particles are widely dispersed inside the microchannel.

Comparing the device performance, we see distinctively better performance with HA and PEO compared to PVP solution. Our analytical calculations, numerical simulations and focusing experiments are all in good agreement. In general, three main focusing methods have been used for 3D focusing: hydrodynamic[101, 102, 103, 65, 66, 67, 71, 104, 105, 106, 107, 108], acoustic[69, 109, 110], and inertial[72, 19, 79, 111] focusing. Although this study presents the first attempt of combining viscoelastic focusing with microflow cytometry, we have achieved good results. Considering the simplicity of the presented system, viscoelastic focusing is a promising approach for sheathless microflow cytometers. Such a system can also be equipped with high-end detection circuitries to match the throughput obtained using state-of-the-art commercial cytometers.

3.7 Conclusion

In this chapter, viscoelastic focusing of microparticles, potential tool for microflow cytometry is demonstrated. We devised a system composed of a straight capillary and optical microscopy. Using the viscoelastic effect, we were able to achieve single-train focusing of microparticles. The performance of three different viscoelastic solutions were analyzed using analytical, numerical and experimental methods. HA and PEO solutions have successful performance in achieving 3D focusing. Using numerical particle tracking, we were able to demonstrate the focusing results at different locations along the microcapillary. It was experimentally verified that $HA_{1.06MDa}$ and PEO_{5MDa} solutions can focus 6 μm diameter particles in a single-line. We have also analyzed the elastic force analytically and quantified the viscoelastic effect using a rheological term that yielded very similar results to our numerical and experimental observations. We investigated the position of particles with optical system and image processing to exhibit trace of particles. Thanks to the simplicity and performance of the focusing technique, it can have a wide range of uses in microflow cytometry applications.

Chapter 4

Summary and Outlook

In this thesis, passive manipulation of particles and cells inside Newtonian and non-Newtonian fluids was investigated. First part of the thesis relates to inertial migration of particles and cells within 2D and 3D systems. To better unravel the physical phenomena of inertial migration, both computational and experimental analysis were carried out. For planar layout, a new structure called squarel was introduced and its performance was compared with the famous spiral design. For both cases, red blood cell focusing was shown visually. For squarel, due to the sharp turns in the corners, strong Dean drag force was created and the balance between this force and inertial lift force determines the focusing region. For both designs, based on the geometrical parameters and flow condition, red blood cells were aligned near the inner wall. To discover unexplored behaviors inside 3D structures, novel fabrication process was presented enabling to construct reconfigurable structures. Consequently, by using this method 3D helical microchannels were constructed.

To understand 3D migration behavior while particles are flowing through the microchannel, computational modeling was developed by using Lagrangian discrete phase model. To consider all of the effective parameters on particles motion, all parameters were analyzed individually. First, the effect of helix diameter was considered and diameters of 2 mm, 8, mm, 14 mm, and 20 mm were analyzed.

It was shown that by increasing the helix diameter, Dean drag force effect on particles motion decreases and relaxing point of the particles move from outer upper part of the cross section towards inner bottom region. Moreover, for small helix diameter, strong Dean drag force rotates particles in an elliptic motion near the inner wall which lowers focusing efficiency. Therefore, an optimized diameter should be chosen for efficient focusing which can be reached by computational modeling analysis. Next, particle size effect on focusing was investigated and it was shown that by decreasing the size of particles, focusing of particles gets worse. This results from weak inertial lift force exerted on the small particles. Next, aspect ratio of the rectangular microchannels was considered. It was shown that by increasing the aspect ratio, the particles need more time and longer length to travel to a stable postion. The interesting part of the analysis is about the helix pitch where increasing the helix pitch resulted in the movement of the upper attractor point towards the outer wall. Moreover, the effect of helix pitch and flow rate were verified by experimental approach.

For the second part of this thesis, manipulation of particles inside non-Newtonian viscoelastic fluids was analyzed. Viscoelastic fluids were prepared by using PEO, HA, and PVP polymers. While PEO and PVP have constant viscosity for the shear rate range of this study, HA illustrates shear thinning behavior. Focusing efficiency of the particles were analyzed by numerical, analytical and experimental approaches. HA and PEO solutions resulted in superior focusing of 6 μm particles. To discover particles size and position, optical image flow cytometry was developed by using optical microscopy and high speed camera. By running the experiment, particle size and and position at the outlet inside HA, PEO, and PVP solution were obtained. For HA and PEO solutions, particles are aligned in a train in the center of the microchannel, however, PVP solution fails in focusing of the particles. Superior performance of HA and PEO in 3D focusing makes them ideal tool for flow cytometry.

Future works of both studies seem surprising. For inertial microfluidics study, due to the capability of "tape'n roll" method to fabricate both 2D and 3D layouts, it can be used to configure microchannels in different orientations. For instance, it is possible to construct two spirals with perpendicular axes of rotation. When

the particles are loaded inside the first spiral, they align in two points near the inner wall of the first spiral. Then, they enter the second spiral with perpendicular axis of rotation while the two focusing points from the previous spiral rest in one of the Dean vortices of the new spiral. Afterward, in the second spiral, it is possible to balance Dean drag force and inertial lift force to focus particles in a single line. This method can be used for variety of applications including optical flow cytometry where single line focusing is critical for cell characterization. For viscoelastic fluids, as it was discussed previously, the main advantage of the elastic lift force to the inertial force is its capability to focus small size particles. Therefore, similar analysis can be done for flow cytometry of nanoparticles using similar but scaled-down microchannels.

Bibliography

[1] D. Di Carlo, D. Irimia, R. G. Tompkins, and M. Toner, "Continuous inertial focusing, ordering, and separation of particles in microchannels," *Proceedings of the National Academy of Sciences*, vol. 104, no. 48, pp. 18892–18897, 2007.

[2] A. A. S. Bhagat, S. S. Kuntaegowdanahalli, and I. Papautsky, "Continuous particle separation in spiral microchannels using dean flows and differential migration," *Lab on a Chip*, vol. 8, no. 11, pp. 1906–1914, 2008.

[3] A. Leshansky, A. Bransky, N. Korin, and U. Dinnar, "Tunable nonlinear viscoelastic "focusing" in a microfluidic device," *Physical review letters*, vol. 98, no. 23, p. 234501, 2007.

[4] G. D'Avino, G. Romeo, M. M. Villone, F. Greco, P. A. Netti, and P. L. Maffettone, "Single line particle focusing induced by viscoelasticity of the suspending liquid: theory, experiments and simulations to design a micropipe flow-focuser," *Lab on a Chip*, vol. 12, no. 9, pp. 1638–1645, 2012.

[5] S. Yang, J. Y. Kim, S. J. Lee, S. S. Lee, and J. M. Kim, "Sheathless elasto-inertial particle focusing and continuous separation in a straight rectangular microchannel," *Lab on a Chip*, vol. 11, no. 2, pp. 266–273, 2011.

[6] A. A. S. Bhagat, H. Bow, H. W. Hou, S. J. Tan, J. Han, and C. T. Lim, "Microfluidics for cell separation," *Medical & biological engineering & computing*, vol. 48, no. 10, pp. 999–1014, 2010.

[7] D. R. Gossett, W. M. Weaver, A. J. Mach, S. C. Hur, H. T. K. Tse, W. Lee, H. Amini, and D. Di Carlo, "Label-free cell separation and sorting in microfluidic systems," *Analytical and bioanalytical chemistry*, vol. 397, no. 8, pp. 3249–3267, 2010.

[8] M. E. Warkiani, A. K. P. Tay, B. L. Khoo, X. Xiaofeng, J. Han, and C. T. Lim, "Malaria detection using inertial microfluidics," *Lab on a Chip*, vol. 15, no. 4, pp. 1101–1109, 2015.

[9] Z. Isiksacan, M. T. Guler, A. Kalantarifard, M. Asghari, and C. Elbuken, "Lab-on-a-chip platforms for disease detection and diagnosis," *Biosensors and Nanotechnology: Applications in Health Care Diagnostics*, pp. 155–181.

[10] Z. Isiksacan, M. Asghari, and C. Elbuken, "A microfluidic erythrocyte sedimentation rate analyzer using rouleaux formation kinetics," *Microfluidics and Nanofluidics*, vol. 21, no. 3, p. 44, 2017.

[11] D. Holmes, H. Morgan, and N. G. Green, "High throughput particle analysis: Combining dielectrophoretic particle focussing with confocal optical detection," *Biosensors and Bioelectronics*, vol. 21, no. 8, pp. 1621–1630, 2006.

[12] Y. Zhao, B. S. Fujimoto, G. D. Jeffries, P. G. Schiro, and D. T. Chiu, "Optical gradient flow focusing," *Optics express*, vol. 15, no. 10, pp. 6167–6176, 2007.

[13] L. Liang and X. Xuan, "Diamagnetic particle focusing using ferromicrofluidics with a single magnet," *Microfluidics and nanofluidics*, vol. 13, no. 4, pp. 637–643, 2012.

[14] J. Shi, S. Yazdi, S.-C. S. Lin, X. Ding, I.-K. Chiang, K. Sharp, and T. J. Huang, "Three-dimensional continuous particle focusing in a microfluidic channel via standing surface acoustic waves (ssaw)," *Lab on a Chip*, vol. 11, no. 14, pp. 2319–2324, 2011.

[15] H. Amini, W. Lee, and D. Di Carlo, "Inertial microfluidic physics," *Lab on a Chip*, vol. 14, no. 15, pp. 2739–2761, 2014.

[16] K. W. Seo, H. J. Byeon, H. K. Huh, and S. J. Lee, "Particle migration and single-line particle focusing in microscale pipe flow of viscoelastic fluids," *RSC Advances*, vol. 4, no. 7, pp. 3512–3520, 2014.

[17] M. Asghari, M. Serhatlioglu, B. Ortaç, M. E. Solmaz, and C. Elbuken, "Sheathless microflow cytometry using viscoelastic fluids," *Scientific reports*, vol. 7, no. 1, p. 12342, 2017.

[18] S. C. Hur, H. T. K. Tse, and D. Di Carlo, "Sheathless inertial cell ordering for extreme throughput flow cytometry," *Lab on a Chip*, vol. 10, no. 3, pp. 274–280, 2010.

[19] X. Wang, H. Gao, N. Dindic, N. Kaval, and I. Papautsky, "A low-cost, plug-and-play inertial microfluidic helical capillary device for high-throughput flow cytometry," *Biomicrofluidics*, vol. 11, no. 1, p. 014107, 2017.

[20] A. S. Rane, J. Rutkauskaite, S. Stavrakis, *et al.*, "High-throughput multi-parametric imaging flow cytometry," *Chem*, vol. 3, no. 4, pp. 588–602, 2017.

[21] S. Kahkeshani, H. Haddadi, and D. Di Carlo, "Preferred interparticle spacings in trains of particles in inertial microchannel flows," *Journal of Fluid Mechanics*, vol. 786, 2016.

[22] J. F. Edd, D. Di Carlo, K. J. Humphry, S. Köster, D. Irimia, D. A. Weitz, and M. Toner, "Controlled encapsulation of single-cells into monodisperse picolitre drops," *Lab on a Chip*, vol. 8, no. 8, pp. 1262–1264, 2008.

[23] R. Khojah, R. Stoutamore, and D. Di Carlo, "Size-tunable microvortex capture of rare cells," *Lab on a Chip*, vol. 17, no. 15, pp. 2542–2549, 2017.

[24] H. Haddadi and D. Di Carlo, "Inertial flow of a dilute suspension over cavities in a microchannel," *Journal of Fluid Mechanics*, vol. 811, pp. 436–467, 2017.

[25] W. C. Lee, A. A. S. Bhagat, S. Huang, K. J. Van Vliet, J. Han, and C. T. Lim, "High-throughput cell cycle synchronization using inertial forces in spiral microchannels," *Lab on a Chip*, vol. 11, no. 7, pp. 1359–1367, 2011.

[26] G. Guan, L. Wu, A. A. Bhagat, Z. Li, P. C. Chen, S. Chao, C. J. Ong, and J. Han, "Spiral microchannel with rectangular and trapezoidal cross-sections for size based particle separation," *Scientific reports*, vol. 3, p. 1475, 2013.

[27] M. E. Warkiani, B. L. Khoo, L. Wu, A. K. P. Tay, A. A. S. Bhagat, J. Han, and C. T. Lim, "Ultra-fast, label-free isolation of circulating tumor cells from blood using spiral microfluidics," *Nature protocols*, vol. 11, no. 1, p. 134, 2016.

[28] S. C. Hur, S.-E. Choi, S. Kwon, and D. D. Carlo, "Inertial focusing of non-spherical microparticles," *Applied Physics Letters*, vol. 99, no. 4, p. 044101, 2011.

[29] M. Masaeli, E. Sollier, H. Amini, W. Mao, K. Camacho, N. Doshi, S. Mitragotri, A. Alexeev, and D. Di Carlo, "Continuous inertial focusing and separation of particles by shape," *Physical Review X*, vol. 2, no. 3, p. 031017, 2012.

[30] S. S. Kuntaegowdanahalli, A. A. S. Bhagat, G. Kumar, and I. Papautsky, "Inertial microfluidics for continuous particle separation in spiral microchannels," *Lab on a Chip*, vol. 9, no. 20, pp. 2973–2980, 2009.

[31] A. Russom, A. K. Gupta, S. Nagrath, D. Di Carlo, J. F. Edd, and M. Toner, "Differential inertial focusing of particles in curved low-aspect-ratio microchannels," *New journal of physics*, vol. 11, no. 7, p. 075025, 2009.

[32] J. Zhang, S. Yan, R. Sluyter, W. Li, G. Alici, and N.-T. Nguyen, "Inertial particle separation by differential equilibrium positions in a symmetrical serpentine micro-channel," *Scientific reports*, vol. 4, p. 4527, 2014.

[33] D. Di Carlo, J. F. Edd, K. J. Humphry, H. A. Stone, and M. Toner, "Particle segregation and dynamics in confined flows," *Physical review letters*, vol. 102, no. 9, p. 094503, 2009.

[34] K. Hood, S. Lee, and M. Roper, "Inertial migration of a rigid sphere in three-dimensional poiseuille flow," *Journal of Fluid Mechanics*, vol. 765, pp. 452–479, 2015.

[35] D. Jiang, W. Tang, N. Xiang, and Z. Ni, "Numerical simulation of particle focusing in a symmetrical serpentine microchannel," *RSC Advances*, vol. 6, no. 62, pp. 57647–57657, 2016.

[36] C. Liu, C. Xue, J. Sun, and G. Hu, "A generalized formula for inertial lift on a sphere in microchannels," *Lab on a Chip*, vol. 16, no. 5, pp. 884–892, 2016.

[37] R. Rasooli, *Modeling of inertial particle flow and entry gas flow in microchannels*. PhD thesis, bilkent university, 2017.

[38] Y.-S. Choi, K.-W. Seo, and S.-J. Lee, "Lateral and cross-lateral focusing of spherical particles in a square microchannel," *Lab on a Chip*, vol. 11, no. 3, pp. 460–465, 2011.

[39] J. Zhou and I. Papautsky, "Fundamentals of inertial focusing in microchannels," *Lab on a Chip*, vol. 13, no. 6, pp. 1121–1132, 2013.

[40] J. Kim, J. Lee, C. Wu, S. Nam, D. Di Carlo, and W. Lee, "Inertial focusing in non-rectangular cross-section microchannels and manipulation of accessible focusing positions," *Lab on a Chip*, vol. 16, no. 6, pp. 992–1001, 2016.

[41] J. S. Choi, Y. Piao, and T. S. Seo, "Fabrication of a circular pdms microchannel for constructing a three-dimensional endothelial cell layer," *Bioprocess and biosystems engineering*, vol. 36, no. 12, pp. 1871–1878, 2013.

[42] J. C. Yeo, C. T. Lim, *et al.*, "Emerging flexible and wearable physical sensing platforms for healthcare and biomedical applications," *Microsystems & Nanoengineering*, vol. 2, p. 16043, 2016.

[43] G. Segre, "Radial particle displacements in poseuille flow of suspensions," *Nature*, vol. 189, pp. 209–210, 1961.

[44] Z. Wu, Y. Chen, M. Wang, and A. J. Chung, "Continuous inertial microparticle and blood cell separation in straight channels with local microstructures," *Lab on a Chip*, vol. 16, no. 3, pp. 532–542, 2016.

[45] H. Amini, E. Sollier, M. Masaeli, Y. Xie, B. Ganapathysubramanian, H. A. Stone, and D. Di Carlo, "Engineering fluid flow using sequenced microstructures," *Nature communications*, vol. 4, p. 1826, 2013.

[46] D. Stoecklein, C.-Y. Wu, K. Owsley, Y. Xie, D. Di Carlo, and B. Ganapathysubramanian, "Micropillar sequence designs for fundamental inertial flow transformations," *Lab on a Chip*, vol. 14, no. 21, pp. 4197–4204, 2014.

[47] Q. Zhao, J. Zhang, S. Yan, D. Yuan, H. Du, G. Alici, and W. Li, "High-throughput sheathless and three-dimensional microparticle focusing using a microchannel with arc-shaped groove arrays," *Scientific reports*, vol. 7, p. 41153, 2017.

[48] J. M. Martel and M. Toner, "Particle focusing in curved microfluidic channels," *Scientific Reports*, vol. 3, p. 3340, 2013.

[49] P. Paiè, F. Bragheri, D. Di Carlo, and R. Osellame, "Particle focusing by 3d inertial microfluidics," *Microsystems & Nanoengineering*, vol. 3, p. 17027, 2017.

[50] W. Lee, D. Kwon, W. Choi, G. Y. Jung, A. K. Au, A. Folch, and S. Jeon, "3d-printed microfluidic device for the detection of pathogenic bacteria using size-based separation in helical channel with trapezoid cross-section," *Scientific reports*, vol. 5, p. 7717, 2015.

[51] W. Xi, F. Kong, J. C. Yeo, L. Yu, S. Sonam, M. Dao, X. Gong, and C. T. Lim, "Soft tubular microfluidics for 2d and 3d applications," *Proceedings of the National Academy of Sciences*, p. 201712195, 2017.

[52] E. S. Asmolov, "The inertial lift on a spherical particle in a plane poiseuille flow at large channel reynolds number," *Journal of Fluid Mechanics*, vol. 381, pp. 63–87, 1999.

[53] K. Hood, S. Kahkeshani, D. Di Carlo, and M. Roper, "Direct measurement of particle inertial migration in rectangular microchannels," *Lab on a Chip*, vol. 16, no. 15, pp. 2840–2850, 2016.

[54] K. Hood, "kthood/inertial-lift-force-rectangle-AR1: First release of inertial lift force rectangle AR1," July 2017.

[55] K. Hood, "kthood/inertial-lift-force-rectangle-AR2: First release of inertial lift force rectangle AR2," July 2017.

[56] K. Hood, "kthood/inertial-lift-force-rectangle-AR4: First release of inertial lift force rectangle AR4," July 2017.

[57] K. Hood, "kthood/inertial-lift-force-rectangle-AR8: First release of inertial lift force rectangle AR8," July 2017.

[58] D. Di Carlo, J. F. Edd, D. Irimia, R. G. Tompkins, and M. Toner, "Equilibrium separation and filtration of particles using differential inertial focusing," *Analytical chemistry*, vol. 80, no. 6, pp. 2204–2211, 2008.

[59] N. Xiang, Z. Shi, W. Tang, D. Huang, X. Zhang, and Z. Ni, "Improved understanding of particle migration modes in spiral inertial microfluidic devices," *Rsc Advances*, vol. 5, no. 94, pp. 77264–77273, 2015.

[60] D. C. Duffy, J. C. McDonald, O. J. Schueller, and G. M. Whitesides, "Rapid prototyping of microfluidic systems in poly (dimethylsiloxane)," *Analytical chemistry*, vol. 70, no. 23, pp. 4974–4984, 1998.

[61] Z. Isiksacan, M. T. Guler, B. Aydogdu, I. Bilican, and C. Elbuken, "Rapid fabrication of microfluidic pdms devices from reusable pdms molds using laser ablation," *Journal of Micromechanics and Microengineering*, vol. 26, no. 3, p. 035008, 2016.

[62] M. V. Hoang, H.-J. Chung, and A. L. Elias, "Irreversible bonding of polyimide and polydimethylsiloxane (pdms) based on a thiol-epoxy click reaction," *Journal of Micromechanics and Microengineering*, vol. 26, no. 10, p. 105019, 2016.

[63] X. Mao, A. A. Nawaz, S.-C. S. Lin, M. I. Lapsley, Y. Zhao, J. P. McCoy, W. S. El-Deiry, and T. J. Huang, "An integrated, multiparametric flow cytometry chip using "microfluidic drifting" based three-dimensional hydrodynamic focusing," *Biomicrofluidics*, vol. 6, no. 2, p. 024113, 2012.

[64] P. Paiè, F. Bragheri, R. M. Vazquez, and R. Osellame, "Straightforward 3d hydrodynamic focusing in femtosecond laser fabricated microfluidic channels," *Lab on a Chip*, vol. 14, no. 11, pp. 1826–1833, 2014.

[65] M. Rosenauer, W. Buchegger, I. Finoulst, P. Verhaert, and M. Vellekoop, "Miniaturized flow cytometer with 3d hydrodynamic particle focusing and integrated optical elements applying silicon photodiodes," *Microfluidics and Nanofluidics*, vol. 10, no. 4, pp. 761–771, 2011.

[66] A. Kummrow, J. Theisen, M. Frankowski, A. Tuchscheerer, H. Yildirim, K. Brattke, M. Schmidt, and J. Neukammer, "Microfluidic structures for flow cytometric analysis of hydrodynamically focussed blood cells fabricated by ultraprecision micromachining," *Lab on a Chip*, vol. 9, no. 7, pp. 972–981, 2009.

[67] M. J. Kennedy, S. J. Stelick, L. G. Sayam, A. Yen, D. Erickson, and C. A. Batt, "Hydrodynamic optical alignment for microflow cytometry," *Lab on a Chip*, vol. 11, no. 6, pp. 1138–1143, 2011.

[68] S. Yan, J. Zhang, M. Li, G. Alici, H. Du, R. Sluyter, and W. Li, "On-chip high-throughput manipulation of particles in a dielectrophoresis-active hydrophoretic focuser," *Scientific reports*, vol. 4, p. 5060, 2014.

[69] Y. Chen, A. A. Nawaz, Y. Zhao, P.-H. Huang, J. P. McCoy, S. J. Levine, L. Wang, and T. J. Huang, "Standing surface acoustic wave (ssaw)-based microfluidic cytometer," *Lab on a Chip*, vol. 14, no. 5, pp. 916–923, 2014.

[70] C. Simonnet and A. Groisman, "Two-dimensional hydrodynamic focusing in a simple microfluidic device," *Applied Physics Letters*, vol. 87, no. 11, p. 114104, 2005.

[71] R. A. Erickson and R. Jimenez, "Microfluidic cytometer for high-throughput measurement of photosynthetic characteristics and lipid accumulation in individual algal cells," *Lab on a Chip*, vol. 13, no. 15, pp. 2893–2901, 2013.

[72] W. Tang, D. Tang, Z. Ni, N. Xiang, and H. Yi, "Microfluidic impedance cytometer with inertial focusing and liquid electrodes for high-throughput cell counting and discrimination," *Analytical chemistry*, vol. 89, no. 5, pp. 3154–3161, 2017.

[73] A. A. S. Bhagat, S. S. Kuntaegowdanahalli, N. Kaval, C. J. Seliskar, and I. Papautsky, "Inertial microfluidics for sheath-less high-throughput flow cytometry," *Biomedical microdevices*, vol. 12, no. 2, pp. 187–195, 2010.

[74] B. Kim and J. M. Kim, "Elasto-inertial particle focusing under the viscoelastic flow of dna solution in a square channel," *Biomicrofluidics*, vol. 10, no. 2, p. 024111, 2016.

[75] J. Nam, B. Namgung, C. T. Lim, J.-E. Bae, H. L. Leo, K. S. Cho, and S. Kim, "Microfluidic device for sheathless particle focusing and separation using a viscoelastic fluid," *Journal of Chromatography A*, vol. 1406, pp. 244–250, 2015.

[76] E. J. Lim, T. J. Ober, J. F. Edd, S. P. Desai, D. Neal, K. W. Bong, P. S. Doyle, G. H. McKinley, and M. Toner, "Inertio-elastic focusing of bioparticles in microchannels at high throughput," *Nature communications*, vol. 5, p. 4120, 2014.

[77] F. Del Giudice, G. Romeo, G. D'Avino, F. Greco, P. A. Netti, and P. L. Maffettone, "Particle alignment in a viscoelastic liquid flowing in a square-shaped microchannel," *Lab on a Chip*, vol. 13, no. 21, pp. 4263–4271, 2013.

[78] J.-P. Matas, J. F. Morris, and É. Guazzelli, "Inertial migration of rigid spherical particles in poiseuille flow," *Journal of Fluid Mechanics*, vol. 515, pp. 171–195, 2004.

[79] A. A. S. Bhagat, S. S. Kuntaegowdanahalli, and I. Papautsky, "Inertial microfluidics for continuous particle filtration and extraction," *Microfluidics and nanofluidics*, vol. 7, no. 2, pp. 217–226, 2009.

[80] D. Li, X. Lu, and X. Xuan, "Viscoelastic separation of particles by size in straight rectangular microchannels: a parametric study for a refined

understanding," *Analytical chemistry*, vol. 88, no. 24, pp. 12303–12309, 2016.

[81] X. Lu and X. Xuan, "Continuous microfluidic particle separation via elasto-inertial pinched flow fractionation," *Analytical chemistry*, vol. 87, no. 12, pp. 6389–6396, 2015.

[82] N. Xiang, X. Zhang, Q. Dai, J. Cheng, K. Chen, and Z. Ni, "Fundamentals of elasto-inertial particle focusing in curved microfluidic channels," *Lab on a Chip*, vol. 16, no. 14, pp. 2626–2635, 2016.

[83] B. Steinhaus, A. Q. Shen, and R. Sureshkumar, "Dynamics of viscoelastic fluid filaments in microfluidic devices," *Physics of Fluids*, vol. 19, no. 7, p. 073103, 2007.

[84] G. Li, G. H. McKinley, and A. M. Ardekani, "Dynamics of particle migration in channel flow of viscoelastic fluids," *Journal of Fluid Mechanics*, vol. 785, pp. 486–505, 2015.

[85] S. H. Yang, D. J. Lee, J. R. Youn, and Y. S. Song, "Multiple-line particle focusing under viscoelastic flow in a microfluidic device," *Analytical chemistry*, vol. 89, no. 6, pp. 3639–3647, 2017.

[86] T. A. Waigh, "Advances in the microrheology of complex fluids," *Reports on Progress in Physics*, vol. 79, no. 7, p. 074601, 2016.

[87] S. J. Haward, A. Jaishankar, M. Oliveira, M. Alves, and G. McKinley, "Extensional flow of hyaluronic acid solutions in an optimized microfluidic cross-slot device," *Biomicrofluidics*, vol. 7, no. 4, p. 044108, 2013.

[88] R. Bird, "Armstrong and rc hassager, o.,"dynamics of polymeric liquids". v. 1," 1987.

[89] B. Ho and L. Leal, "Migration of rigid spheres in a two-dimensional unidirectional shear flow of a second-order fluid," *Journal of Fluid Mechanics*, vol. 76, no. 4, pp. 783–799, 1976.

[90] D. F. James, "Boger fluids," *Annual Review of Fluid Mechanics*, vol. 41, pp. 129–142, 2009.

[91] M. Tehrani, "An experimental study of particle migration in pipe flow of viscoelastic fluids," *Journal of Rheology*, vol. 40, no. 6, pp. 1057–1077, 1996.

[92] K. Kang, S. S. Lee, K. Hyun, S. J. Lee, and J. M. Kim, "Dna-based highly tunable particle focuser," *Nature communications*, vol. 4, p. 2567, 2013.

[93] A. S. Basu, "Droplet morphometry and velocimetry (dmv): a video processing software for time-resolved, label-free tracking of droplet parameters," *Lab on a Chip*, vol. 13, no. 10, pp. 1892–1901, 2013.

[94] V. A. Martinez, J. Schwarz-Linek, M. Reufer, L. G. Wilson, A. N. Morozov, and W. C. Poon, "Flagellated bacterial motility in polymer solutions," *Proceedings of the National Academy of Sciences*, vol. 111, no. 50, pp. 17771–17776, 2014.

[95] V. Can and O. Okay, "Shake gels based on laponite–peo mixtures: effect of polymer molecular weight," *Designed monomers and polymers*, vol. 8, no. 5, pp. 453–462, 2005.

[96] R. Mendichi, L. Šoltés, and A. Giacometti Schieroni, "Evaluation of radius of gyration and intrinsic viscosity molar mass dependence and stiffness of hyaluronan," *Biomacromolecules*, vol. 4, no. 6, pp. 1805–1810, 2003.

[97] J. Claverie, *Polymers in Dispersed Media I: International Conference on Polymers in Dispersed Media*, vol. 1. John Wiley & Sons, 2000.

[98] W. W. Graessley, "Polymer chain dimensions and the dependence of viscoelastic properties on concentration, molecular weight and solvent power," *Polymer*, vol. 21, no. 3, pp. 258–262, 1980.

[99] V. Tirtaatmadja, G. H. McKinley, and J. J. Cooper-White, "Drop formation and breakup of low viscosity elastic fluids: Effects of molecular weight and concentration," *Physics of fluids*, vol. 18, no. 4, p. 043101, 2006.

[100] S. Shimabayashi, T. Sannoh, and M. Nakagaki, "Decrease in intrinsic viscosity of polyvinylpyrrolidone in the presence of sodium chondroitin sulfate or sodium carboxymethylcellulose in an aqueous solution," *Chemical and pharmaceutical bulletin*, vol. 37, no. 10, pp. 2811–2813, 1989.

[101] M. Serhatlioglu, C. Elbuken, B. Ortac, and M. E. Solmaz, "Femtosecond laser fabrication of fiber based optofluidic platform for flow cytometry applications," in *Optical Fibers and Sensors for Medical Diagnostics and Treatment Applications XVII*, vol. 10058, p. 100580I, International Society for Optics and Photonics, 2017.

[102] Y. Zhao, Q. Li, X. Hu, and Y. Lo, "Microfluidic cytometers with integrated on-chip optical systems for red blood cell and platelet counting," *Biomicrofluidics*, vol. 10, no. 6, p. 064119, 2016.

[103] B. R. Watts, Z. Zhang, C. Q. Xu, X. Cao, and M. Lin, "A photonic-microfluidic integrated device for reliable fluorescence detection and counting," *Electrophoresis*, vol. 33, no. 21, pp. 3236–3244, 2012.

[104] Z. Cheng, X. Wu, J. Cheng, and P. Liu, "Microfluidic fluorescence-activated cell sorting (μfacs) chip with integrated piezoelectric actuators for low-cost mammalian cell enrichment," *Microfluidics and Nanofluidics*, vol. 21, no. 1, p. 9, 2017.

[105] G. Testa, G. Persichetti, and R. Bernini, "Micro flow cytometer with self-aligned 3d hydrodynamic focusing," *Biomedical optics express*, vol. 6, no. 1, pp. 54–62, 2015.

[106] M. Frankowski, N. Bock, A. Kummrow, S. Schädel-Ebner, M. Schmidt, A. Tuchscheerer, and J. Neukammer, "A microflow cytometer exploited for the immunological differentiation of leukocytes," *Cytometry Part A*, vol. 79, no. 8, pp. 613–624, 2011.

[107] C. Simonnet and A. Groisman, "High-throughput and high-resolution flow cytometry in molded microfluidic devices," *Analytical chemistry*, vol. 78, no. 16, pp. 5653–5663, 2006.

[108] H. Bang, H. Yun, W. G. Lee, J. Park, J. Lee, S. Chung, K. Cho, C. Chung, D.-C. Han, and J. K. Chang, "Expansion channel for microchip flow cytometers," *Lab on a Chip*, vol. 6, no. 10, pp. 1381–1383, 2006.

[109] G. Goddard, J. C. Martin, S. W. Graves, and G. Kaduchak, "Ultrasonic particle-concentration for sheathless focusing of particles for analysis in a flow cytometer," *cytometry part A*, vol. 69, no. 2, pp. 66–74, 2006.

[110] G. R. Goddard, C. K. Sanders, J. C. Martin, G. Kaduchak, and S. W. Graves, "Analytical performance of an ultrasonic particle focusing flow cytometer," *Analytical chemistry*, vol. 79, no. 22, pp. 8740–8746, 2007.

[111] J. Oakey, R. W. Applegate Jr, E. Arellano, D. D. Carlo, S. W. Graves, and M. Toner, "Particle focusing in staged inertial microfluidic devices for flow cytometry," *Analytical chemistry*, vol. 82, no. 9, pp. 3862–3867, 2010.

Appendix A

Supplementary Figures

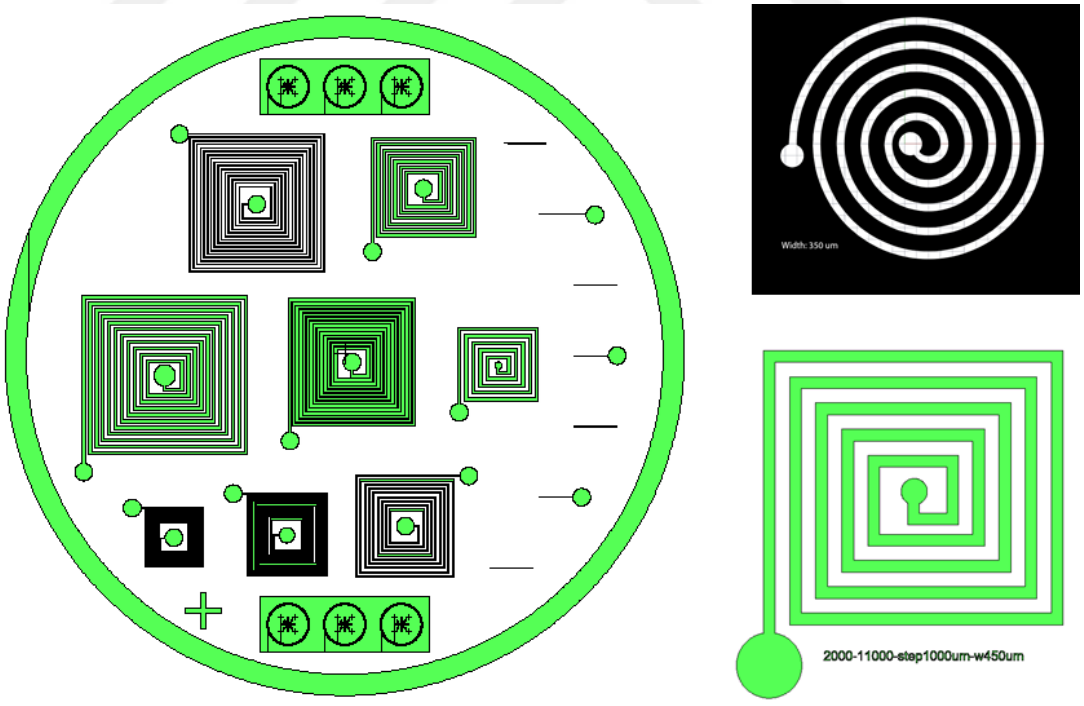

Figure A.1: Mold designs used for investigating inertial migration in planar structures

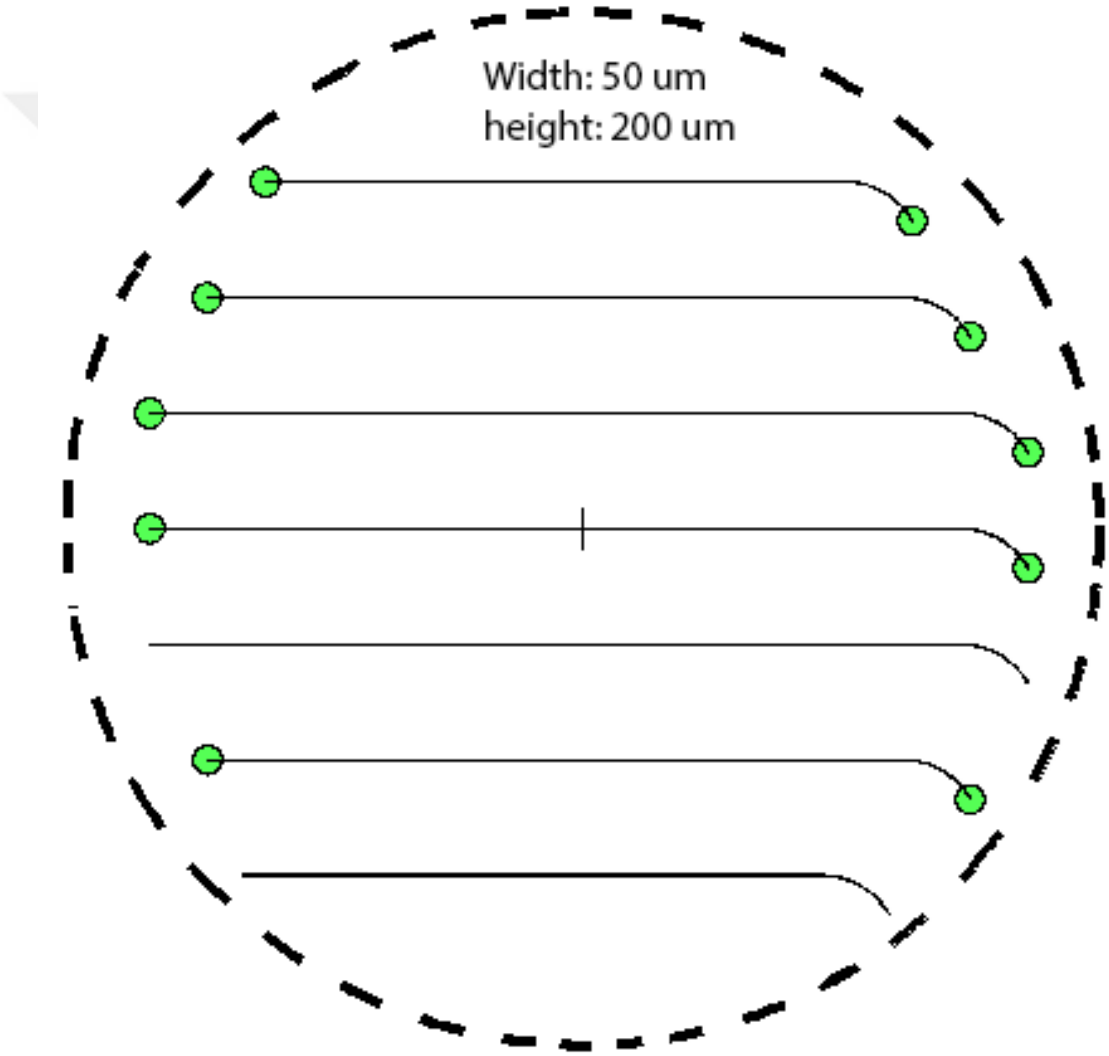

Figure A.2: Mold design used for fabrication of helical microchannel